DEVELOPMENT OF MONOLAYER MoS_2 BASED ENZYME SENSORS

Master of Science Thesis

Cem ODACI

Eskişehir, 2019

DEVELOPMENT OF MONOLAYER MoS_2 BASED ENZYME SENSORS

Cem ODACI

MASTER OF SCIENCE THESIS

Department of Electrical and Electronics Engineering

Supervisor: Assoc. Prof. Dr. Feridun AY

Eskişehir

Eskişehir Technical University

Institute of Graduate Programs

August 2019

This work was supported by the Scientific and Technological Research Council of Turkey (TÜBİTAK), with the project numbers of 114E594 and 116F445. It is also supported by the Scientific Research Project Council (BAP), project no BAP1801F020.

FINAL APPROVAL FOR THESIS

This thesis titled "Development of Monolayer MoS_2 Based Enzyme Sensors" has been prepared and submitted by Cem ODACI in partial fulfillment of the requirements in "Eskişehir Technical University Directive on Graduate Education and Examination" for the Degree of Master of Science in Electrical and Electronics Engineering Department has been examined and approved on 08/08/2019.

Committee Members	**Title Name Surname**	**Signature**
Member(Supervisor)	: Assoc. Prof. Dr. Feridun AY	.....
Member	: Assoc. Prof. Dr. Nihan KOSKU PERKGÖZ	.....
Member	: Assoc. Prof. Dr. Urartu Özgür Şafak ŞEKER	.....
Member	: Dr. Suzan Biran AY	.....
Member	: Dr. Yasemin ÇELİK	.....

Prof. Dr. Murat TANIŞLI
Director of Graduate School of Sciences

ABSTRACT

DEVELOPMENT OF MONOLAYER MoS_2 BASED ENZYME SENSORS

CEM ODACI

Department of Electrical and Electronics Engineering

Eskişehir Technical University, Graduate School of Science, 6.2018

Supervisor: Assoc. Prof. Dr. Feridun AY

Two-dimensional transition metal dichalcogenide (TMDC) materials have attracted an important deal of interest in electronic, photonic and optoelectronic applications depending on their unique structural properties. Recently, they are also utilized in biosensor applications for different purposes such as diagnosis, detection, sensing of the microorganisms, proteins, gases, etc. In this thesis, the photonic and electronic investigation of the horseradish peroxidase (HRP) enzyme with the interaction of the monolayer MoS_2 flakes is studied. Monolayer MoS_2 flakes are grown by chemical vapor deposition method with the help of the controllable vacuum system. Optical microscopy, Raman spectroscopy, and atomic force microscopy tools are used for the characterization of the grown MoS_2 flakes. After that, for the analysis of the interaction of the enzyme and MoS_2 flakes, it is focused on the photoluminescence (PL) and Raman spectrum measurements. The changes on the PL and Raman spectra are observed and interpreted. Followingly, I-V measurements of the interaction between the enzyme and MoS_2 flakes are performed and the variations with respect to this interaction are attempted to clarify. We believe that this work can be an executive support for the future studies related to the interactions between TMDC materials and enzyme solutions for the detection, diagnosis, etc.

Keywords: Transition metal dichalcogenide, Chemical vapor deposition, Enzyme, Monolayer, MoS_2

ÖZET

TEK KATMANLI MoS_2 TABANLI ENZİM SENSÖRLERİNİN GELİŞTİRİLMESİ

Cem ODACI

Elektrik-Elektronik Mühendisliği Anabilim Dalı

Eskişehir Teknik Üniversitesi, Fen Bilimleri Enstitüsü, 6.2018

Danışman: Doç. Dr. Feridun AY

İki boyutlu geçiş metal dikalkogenit (GMD) malzemeleri, eşsiz yapısal özelliklerine bağlı olarak, fotonik, elektronik ve opto-elektronik uygulamalarında önemli derecede dikkat çekmektedir. Son zamanlarda, bu iki boyutlu malzemeler, gazların, proteinlerin, mikroorganizmaların teşhisi, algılanması ve sezilmesi gibi farklı amaçlar için biyosensör uygulamalarında da kullanılabilmektedir. Bu tezde, tek katmanlı MoS_2 yapılarının horseradish peroxidase (HRP) enzimi ile etkileşiminin, elektronik ve fotonik araştırması yapılmıştır. Tek katmanlı MoS_2 yapıları kontrollü vakum sistemine sahip kimyasal buhar biriktirme yöntemiyle üretilmiştir. Üretilen bu yapılar, optik mikroskop, Raman spektroskopisi ve atomik kuvvet mikroskobu kullanılarak karakterize edilmiştir. Daha sonra, MoS_2 yapılarının ve enzim solüsyonunun etkileşiminin analizini yapmak için, fotolüminesans ve Raman spektrumları üzerinde odaklanılmıştır. PL ve Raman spektrumlarındaki değişimler gözlemlenmiştir ve yorumlanmıştır. Takiben, enzim ve MoS_2 yapılarının etkileşiminin I-V ölçümleri gerçekleştirilmiştir ve etkileşime bağlı olarak meydana gelen değişimler açıklanmaya çalışılmıştır. Bu çalışmanın, geçiş metal dikalkogenitler ile enzim solüsyonları arasındaki etkileşimlerin incelenmesi üzerine gelecekte yapılacak çalışmalar için önemli bir destek sağlayacağına inanmaktayız.

Anahtar Sözcükler: Geçiş metal dikalkogenit, Kimyasal buhar biriktirme, MoS_2, enzim, tek katman

08/08/2019

STATEMENT OF COMPLIANCE WITH ETHICAL PRINCIPLES AND RULES

I hereby truthfully declare that this thesis is an original work prepared by me; that I have behaved in accordance with the scientific ethical principles and rules throughout the stages of preparation, data collection, analysis and presentation of my work; that I have cited the sources of all the data and information that could be obtained within the scope of this study, and included these sources in the references section; and that this study has been scanned for plagiarism with "scientific plagiarism detection program" used by Eskişehir Technical University, and that "it does not have any plagiarism" whatsoever. I also declare that, if a case contrary to my declaration is detected in my work at any time, I hereby express my consent to all the ethical and legal consequences that are involved.

Cem ODACI

ACKNOWLEDGMENT

The work presented in this thesis has been carried out from September 2016 to August 2019, under the supervision of Assoc. Prof. Feridun AY. All the work performed in this thesis has been possible with the help of the kind and hardworking people in the MIDAS research group. I will always be thankful.

First of all, I would like to thank to my advisor, Assoc. Prof. Dr. Feridun Ay, for giving me such an opportunity and allowing me to join in his research group. I was very fortunate to have such an inspiring and understanding advisor, who has made my graduate study fruitful. Along with the encouragement, training and support that he gave me in science, I also deeply appreciate his willingness to care about students' life beyond the work. His wisdom and open mindedness to balance work and life have set him as a role model for me. I could not ask for better advisor than him.

I would like to also thank to Assoc. Prof. Dr. Nihan Kosku PERKGÖZ and Dr. Suzan Biran AY for supporting me and giving me instructions about my experiments during my work in the both Micro/Nano Devices and Systems Laboratory in the department of the Electrical-Electronic Engineering and Biotechnology Laboratory in the department of the Chemical Engineering.

Also, I especially thank to my thesis committee members (Assoc. Prof. Dr. Feridun Ay, Assoc. Prof. Dr. Nihan Kosku PERKGÖZ, Assoc. Prof. Dr. Urartu Özgür Şafak ŞEKER, Dr. Suzan Biran AY, Dr. Yasemin ÇELİK) for making time to attend my presentation and their valuable criticism related to my thesis.

I would like to thank to also my friends and colleagues in the MİDAS research group (Res. Asst. Mustafa DEMİRTAŞ, Res. Asst. Hüseyin ŞAR, Res. Asst. Gonca Uslu ÖZKÜÇÜK, Dr. Ayberk ÖZDEN, Ezgi ŞAHİN, Büşra YORULMAZ, Merve ÖPER) for their supports and contributions on my experiments and measurements. Also, I am grateful for their kindness and friendliness. I also appreciate their knowledge and encouragement that they have given me during graduate study.

Finally, I especially would love to thank to my parents and brothers for all their support, encouragements and love that have been the constant in my whole life.

Cem ODACI

08.08.2019

Eskişehir, Turkey

TABLE OF CONTENTS

Page

Page

LIST OF FIGURES

Page

Page

Page

Page

LIST OF TABLES

Page

LIST OF ABBREVIATIONS

AFM: Atomic Force Microscopy

ALD: Atomic Layer Deposition

CVD: Chemical Vapor Deposition

DI: Deionized

FET: Field Effect Transistor

FTIR: Fourier Transform Infrared Spectroscopy

FWHM: Full Width Half Maximum

HRP: Horseradish Peroxidase

ISFET: Ion-sensitive Field Effect Transistor

LED: Light Emitting Diode

LCV: Leuco Crystal Violet

MOSFET: Metal-oxide-semiconductor Field Effect Transistor

PL: Photoluminescence

TMDC: Transition Metal Dichalcogenide

1. INTRODUCTION

Two-dimensional (2D) materials has been interested to provide higher packing density, faster circuit speed, and lower power dissipation. Since the miniaturization of the silicon-based electronic devices is approaching to the physical limits for their operations [1], 2D TMDC materials have been attracted too much attention on the respect of their unique properties since the discovery of the graphene. Even though there were theoretical studies of graphene, scientists could not isolate monolayer sheet of graphene until 2004 [2]. This occasion has emerged a growing research at an enormous rate on 2D materials.

2D or a layered shaped material is had when one dimension is restricted. A wired or 1D material is had when two dimensions are size-limited. As all dimensions are restricted in the range of a few nanometers, 0D material is had. Graphene can be shaped in all three dimensions.

1.1. Graphene

Graphene is known as the first two-dimensional atomic crystal with extreme properties [3]. It is composed of hexagonal arrangement of carbon atoms [4]. Also, graphene can be used to obtain carbon nanotubes and fullerenes. Fullerenes are consisted of wrapped graphene and carbon nanotubes are obtained by rolling graphene in a given direction. Fullerenes and carbon nanotubes are zero- and one-dimensional objects, respectively [5].

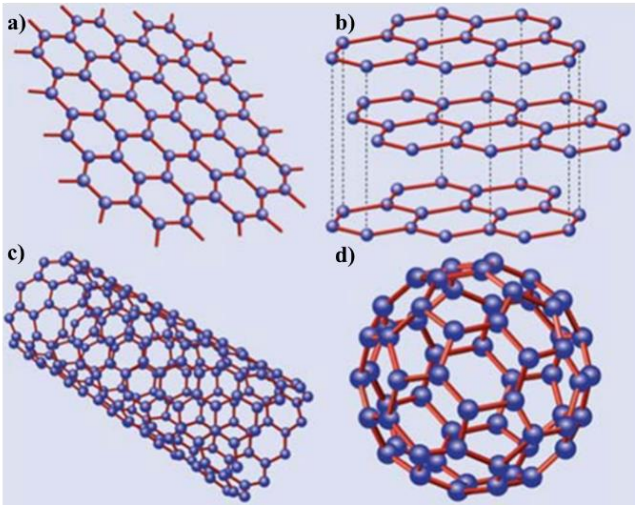

Figure 1.1. *The illustration of a) graphene nanosheet (2D), b) graphite (3D), c) carbon nanotube (1D), d) fullerene (0D)*

Graphene has surpassing characteristics in terms of optical absorption (2.3%), mechanical strength (a Young modulus of 1 TPa and intrinsic strength of 130 GPa), electron mobility ($2.5x10^5$ $cm^2V^{-1}s^{-1}$ at the room-temperature), and thermal conductivity (above 3000 WmK^{-1}) when it is compared to other materials. It also has extrinsic properties such as complete impermeability to any gases and ability to sustain extremely high densities of electric current [3,6]. Along with, since there is a small overlap between conduction band and valence band of the graphene, it shows typical semimetal properties. Without providing any heat, with lower energy, the electrons at the top of the valence band could flow into the bottom of the conduction band [6].

Since graphene has no band gap, the applications have been limited for semiconductor electronics. Researchers searched for other alternatives with similar properties with high carrier mobility and feasible on/off ratio [7].

1.2. Transition Metal Dichalcogenides

Two-dimensional transition metal dichalcogenides (TMDCs) are chemically composed of a transition metal of groups 4-10 (M) and a chalcogen (X) in the form of MX_2. In 3D structures of TMDCs, while there is a covalent bonding of tri-layers, neighboring sheets are bonded via Van der Waals interactions [8]. 2D TMDCs exhibit extreme electrical and optical properties which evolve from quantum confinement and surface effect arisen by the transition of an indirect bandgap to a direct band gap which

means bulk TMDCs are scaled down to monolayers. A strong photoluminescence and high exciton binding energy are originated from this tunable bandgap in TMDC materials, which makes them a promising candidate for the applications in various opto-electronic devices such as solar cells, photo-detectors, light emitting diodes (LEDs), and photo-transistors [9].

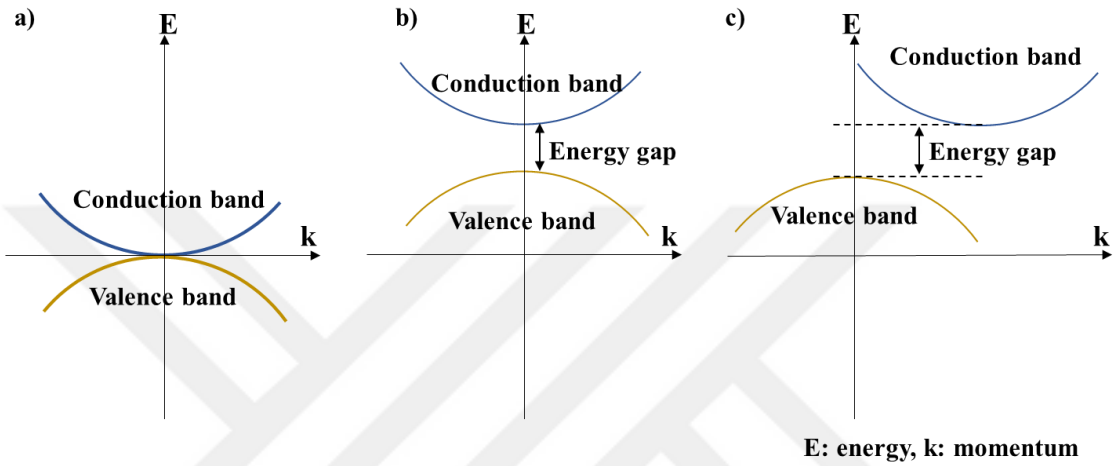

Figure 1.2. *a) There is no band gap (graphene), b) Direct band gap (2D TMDCs), c) Indirect band gap (3D TMDCs)*

There are many types of 2D TMDC materials with diverse properties such as metal (ScS_2, VSe_2), half-metal (MnS_2, $TiSe_2$), and semiconductor (MoS_2, $MoSe_2$, WS_2) [8].

MoS_2

2D MoS_2 is a very promising material for device application among TMDCs due to its perfect gate control, high current capability, scalability. Monolayer MoS_2 has a wide direct band gap which helps it to exhibit good electrical and transport properties, chemical and thermal stability, transparency, and flexibility [1].

A single layer of molybdenum disulfide (MoS_2) is composed of a transition metal, Mo, and a chalcogen, S by a strong ionic bonding [10]. The interaction of multiple layers with weak van der Walls bonding between the adjacent layers originates bulk MoS_2. The thickness of each layer is generally ~0.65 nm [11]. MoS_2 material has a tunable band gap with respect to the number of the layers of the material. It corresponds to 1.2 eV when it is bulk and indirect; and 1.9 eV when it is monolayer and direct [1,12], which opens up

the way for many device applications. It is demonstrated that at the room temperature monolayer MoS_2-based FET exhibit on-off ratio exceeding 10^8 and mobility of ~200 $cm^2V^{-1}s^{-1}$ by using semiconductor MoS_2 as a conductive channel and HfO_2 as a gate channel [13]. Also, MoS_2-based photodetectors can exhibit an advanced responsivity and selectivity in comparison to graphene-based ones [14]. It is found that the maximum photoresponsivity of single layer MoS_2-based photodetector is 880 A/W at a wavelength of 561 nm [15].

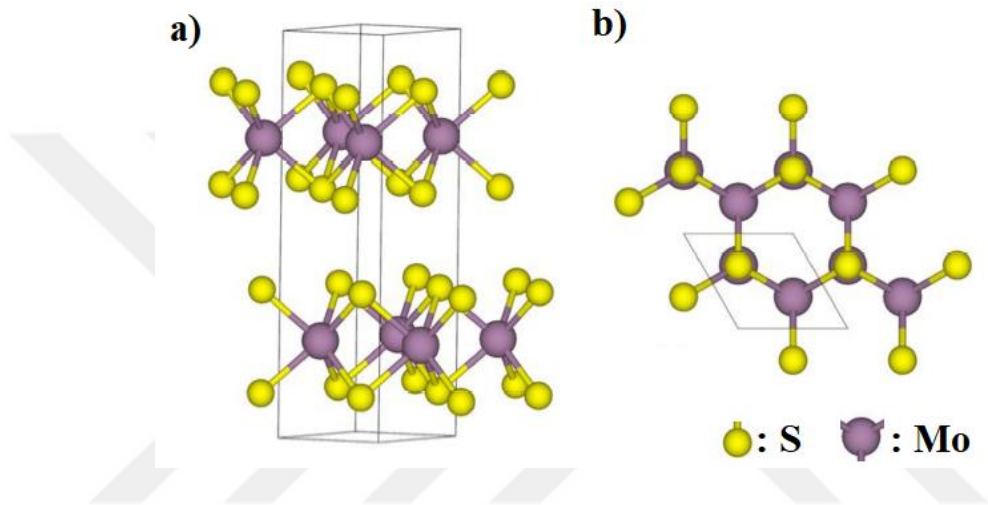

Figure 1.3. *a) The layered structure of MoS_2, and b) monolayer structure of MoS_2 [1]*

WS_2

Tungsten disulfide is another representing member of the semiconducting TMDCs family. It is composed of a transition metal, W, and a chalcogen, S, in the formula of WS_2. In the monolayer WS_2 structure, W atoms are hexagonally sandwiched by two trigonal coordinated S atoms. As the thickness of WS_2 decreases, the bandgap shifts from indirect (bulk) to direct (single layer). It is a semiconducting material with a tunable band gap in the range of 1.4 eV (in bulk) to 2.1 eV (in monolayer) [16].

Monolayer WS_2 is having great attention due to its extreme properties such as high emission quantum yield and large exciton/trion binding energy. It also attracts many interests due to its strong-spin coupling induced valence band splitting, which ensues spin-valley coupling. For MoS_2 structure, the valence band splitting is ~150 meV. For WS_2 structure, it is almost three-times higher (~426 meV) owing to the larger mass of W atoms.

$MoSe_2$

Some studies have indicated that selenide compounds might be superior compared to sulfides because they have a narrower band gap (1.5 eV in $MoSe_2$ and 1.9 eV in MoS_2), which results in a 10-folded narrower line width and tunable excitonic charging effect. Similar to the other TMDCs, changing the layer number of $MoSe_2$ changes its band structure. The band gap increases form bulk (1.1 eV) to monolayer (1.5 eV). This tunability of $MoSe_2$ structure makes it a promising candidate for electrical and optical applications. It is shown that obtaining $MoSe_2$-based transistor with high on/off ratio (10^6) and intrinsic mobility up to 50 $cm^2V^{-1}s^{-1}$ can be achieved [17]. It is also demonstrated that monolayer $MoSe_2$ structures exhibit much faster response time (<25 ms) in comparison to MoS_2 [18].

WSe_2

Tungsten diselenide (WSe_2) is another important member of TMDCs family. It has a similar composition with other TMDC materials, MoS_2, $MoSe_2$, WS_2. W atoms are covalently bonded to S atoms in monolayer WSe_2. Monolayer WSe_2 possesses a direct band gap of ~1.65 eV while bulk has the indirect band gap of ~1.2 eV [19]. Layered WSe_2 exhibits much less light emission than monolayer which is due to the band gap transition in the WSe_2 structure depending on the thickness changes [20]. It is also demonstrated that WSe_2 material is the first TMDC material which is consisted of the combination of p-type and n-type conducting behaviors in the same material. This important property offers the possibility so as to design complementary logic circuits in the same monolayer WSe_2 structure [21]. The applicability of WSe_2 to logic-circuit integrations is shown by WSe_2-based resistor-loaded inverter with a gain of ~13 [22]. It is also proven that monolayer p-type WSe_2-based FETs show splendid electronic characteristics with effective hole carrier mobility up to 100 $cm^2V^{-1}s^{-1}$ at room temperature [20].

1.1. Synthesis of 2D Materials

One of the very substantial research field of TMDCs is to be able to have reliable production of atomically thin 2D layers and their manipulation of the electronic properties by scalable approaches. Two essential strategies have been used to obtain monolayer TMDCs. One of which is the chemical or mechanical exfoliation from bulk structures; the other one is the bottom-up growth method [23]. Some of the top-down and bottom-

up methods are classified in detail in Figure 4 [24]. Based on the processes involved in having nanometer-sized structures, these two different synthesis methods can be distinguished. In bottom-up method, atomic or molecular precursors which reacts and grows in size and self-assemble into more complex structures are used to construct nanoscale materials. Contrarily, the top-down method, large or bulk solids are carved to have nanoscale structures by controlled removal of materials. The top-down method is a useful way to produce high-quality and micrometer-sized monolayer structures. In general, it is persuaded that the mechanically exfoliated monolayer TMDCs have higher quality and cleaner surfaces and are appropriate for fundamental research and the device fabrication in proof-of-concept. Despite this, mechanical cleavage is not a good way to have a large-scale production because of the absence of the controllability of the layer number. Instead, the liquid-phase preparation method is a reliable way for chemical exfoliation of the monolayer TMDCs. In this exfoliation approach, materials are promising for printable or solution-based electronics. However, the wet chemical approach can ineluctably change the lattice structure of thin TMDCs or introduce some defects into structures during the exfoliation process. Thus, this method may require a post treatment to reconstruct the TMDC structures [23,25].

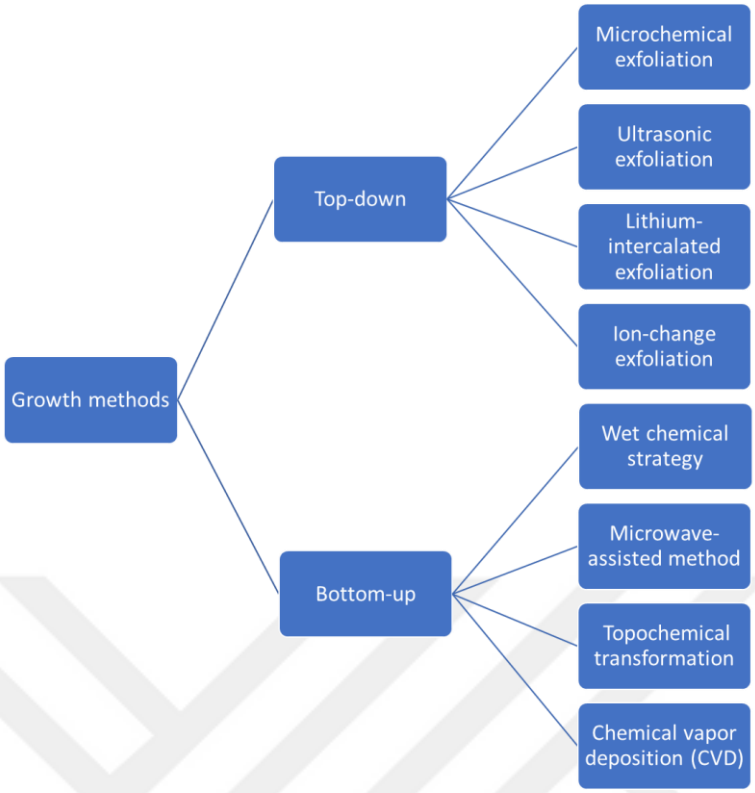

Figure 1.4. *The schematic of the growth methods used for the synthesis of 2D materials*

Some of the growth methods will be briefly mentioned in the following sections.

1.1.1. Top-down synthesis approach

TMDC flakes has a strong covalent bonding between the M (transition metal) and X (chalcogen) atoms. When they are in a layered structure, there possesses weak van der Waal bonds between the layers. As a shear force is imparted to the bulk structure, the weak van der Waals forces can be overcome within the crystal lattice and obtain thinner materials. The lamellar flakes can be exfoliated further by repeating thinning process and at the end single layer nanosheets can be isolated [26]. When micromechanical exfoliation approach is used, a peeling force is applied to separate the layers, which is either a shear-induced separation or compressive delamination. In general, by applying a vibrational energy to the crystal structure or exposing it to forces generated within cavitation field, exfoliation in a liquid medium can be operated. Chemical exfoliation or intercalation avails in regard to the insertion of a small atom or molecule within the interlayer space of the TMDC bulk before the crystal are separated by the forced expansion of the intercalate.

Moreover, to be able to produce a mono- or few-layered nanosheets on a substrate, thinning by etching techniques also requires the destructive removal of unwanted layers from a bulk structure [27].

Some of the drawbacks of these exfoliation methods are [28]:

- low yield,
- uncontrollable layer number,
- relatively small layer number,
- possible defects and phase transformations,
- Non-massive production.

1.1.2. Bottom-up synthesis approach

Even though the mass production by the top-down method is generally very low, it is a useful method to prepare ultrathin nanosheets with high-quality. Also, all of the exfoliation approaches are convenient to the materials of the layered bulk crystals [27]. For practical device applications, to synthesis atomically thin TMDCs with layer controllability and large-area uniformity is an imperative requirement [23]. When bottom-up methods are used, nanoscale materials are produced by the help of atomic or molecular precursors which are proper to react with each other and grow in size. Even, more complex structures can be self-assembled [24].

Herein, we will be focusing on the chemical vapor deposition (CVD) growth method which is one of the synthesis method for 2D TMDC materials among bottom-up approaches.

1.1.2.1. Chemical vapor deposition (CVD) method

CVD method is another appealing strategy for growing single-layer crystalline 2D sheets with high-quality, scalable size, and controllable thickness [27]. The grown TMDC monolayers or films can be used as active components and the building blocks for nanoelectronics and the construction of the layered heterostructures, separately. Presently, the CVD method is the only appropriate way to be able to achieve wafer-scale TMDCs growth [23]. CVD method is a chemical synthesis process with high-temperature, which any desirable material can be grown on substrates [24].

The vapor of the precursors can be introduced from outside or generated inside the quartz tube inside the furnace (Figure 5). The access to high-quality and high purity 2D materials with controllable manners, which allow to control the morphology, crystallinity, and defects of 2D nanostructures by tuning the parameters of the process, are the main benefits of CVD growth process. CVD synthesis process is also another annealing strategy to be able grow the high-quality single-crystalline 2D nanosheets on substrates [23,24].

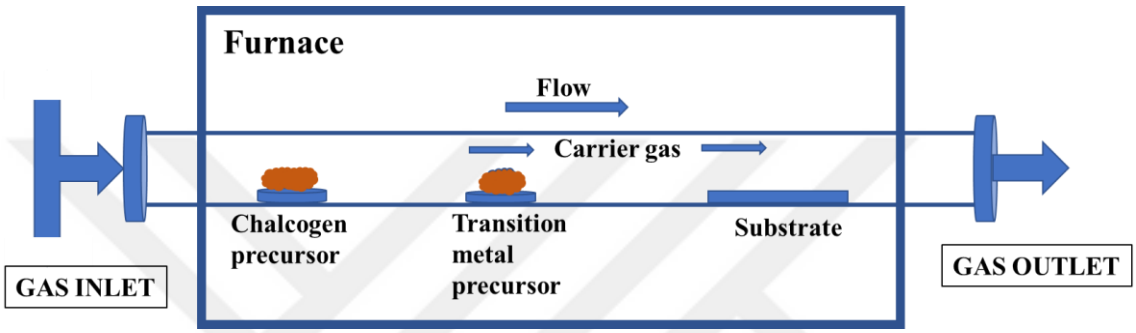

Figure 1.5. *The schematic illustration of the CVD process*

There are some optional ways to take advantages of CVD growth method [23]:

I) Sulfurization (or selenization) of metal (or metal oxide) thin films [29],

II) Thermal decomposition of thiosalts [30],

III) Vapor phase reaction of transition metal oxides with chalcogen precursor [31],

IV) Vapor phase transport and recrystallization from TMD powder [32].

1.1.2.2. Atomic Layer Deposition (ALD)

Atomic layer deposition (ALD) method is a kind of chemical vapor deposition technique. Here, sequential exposures of reactants in the gas phase are used to grow thin films with atomic layer accuracy. Also, it is a very promising growth technique to deposit high-K materials in a very qualitative manner [33]. The self-limiting deposition mechanism of ALD brings out some advantages [34,35]:

I) Accurate and simple thickness controllability, which is only determined by the number of the cycles of the reaction,

II) It is capable of large area deposition,

III) It has an excellent controllability and reproducibility, and less need of flux homogeneity of the reactant unlike CVD.

In ALD method, film deposition occurs in a cyclic manner. In general, one cycle originates in four steps:

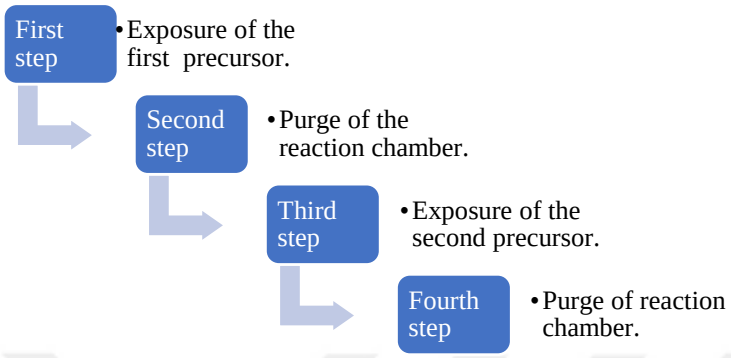

These deposition cycles are repeated as many times as needed to reach the desired thickness of the film. The thickness of the film obtained per cycle may also be based on the size of the precursor molecule due to the fact that steric hindrance between large precursors limits the number of the molecules adsorbed on the surface. However, it is possible to obtain monolayer deposition per cycle in terms of small molecules or elements as precursors [34].

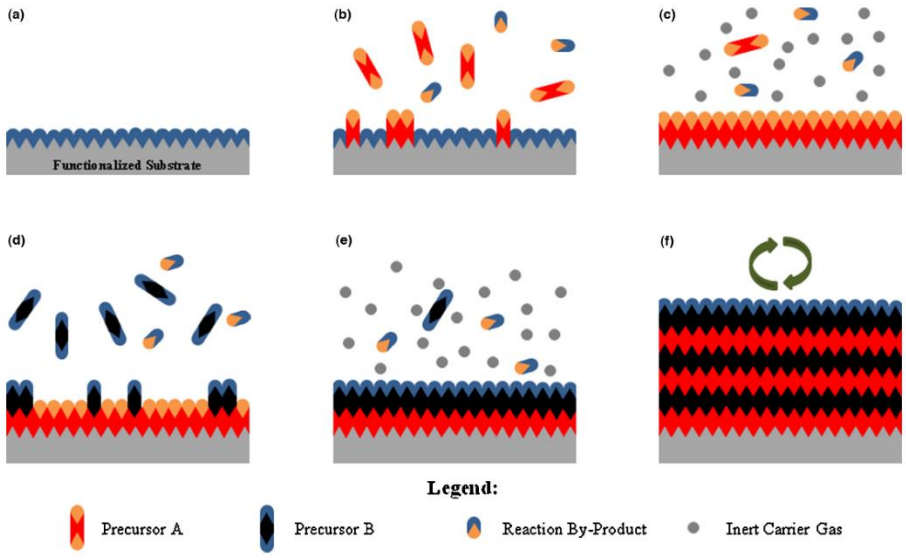

Figure 1.6. *The schematic illustration of ALD process. a) surface functionalization of the substrate. b) Precursor A is pulsed and reacts with the surface of the substrate. c) By the help of inert gas, excess precursors and by products are carried out of the reaction chamber by purging. d) Precursor B is pulsed and reacts with the new surface. e) By purging inert gas, excess precursors and by products carried out of the chamber[36]*

1.2. Characterization of 2D Materials

To ensure the quality, number of the layers, surface homogeneity and thickness of the grown TMDC materials, many characterization tools can be used such as optical microscopy, Raman spectroscopy, Fourier transformation infrared spectroscopy (FTIR), and atomic force microscopy (AFM). In the following sub-sections, these characterization methods are concisely mentioned.

1.2.1. Optical microscopy

The whole surface coverage is the unique characteristic of all of the atomically thick 2D materials. This property allows the tailoring of electronic characteristics for the future applications through favorable engineering processes. However, due to the fact that some undesired environmental factors, which might be a surface contamination, can be problematic, it limits the prospects of the realistic commercialization. Optical spectroscopy tools such as Raman and infrared spectroscopies have had an important role in understanding the compositions and structures of the chemicals [37,38].

These optical microscopy tools are used to visualize and probe the disorders present in the 2D materials and help to reveal several lattice defects. These defects are referred to be uniformity or breakages. These can include vacancy defects, grain boundaries, edge defects, and corrugations. Also, contamination is a real manner in the commercialization of 2D materials. Surface contaminations may be formed form ambient conditions or processing of these materials. Defects or surface contaminations may cause a drastic decrease in the supreme properties of the 2D materials. Nanoscale spectroscopy which provides fast, non-destructive, and reliable measurements is required to understand both defects and contaminants in atomically thin 2D materials [38].

1.2.2. Raman spectroscopy

Raman spectroscopy functions by measuring the frequency shift of inelastically scattered light from the interaction with the sample based on the its unique vibrational characteristic. This vibration has the feature of being fingerprints for each sample itself.

When an incident light is scattered from the sample or by a medium subject to the interaction between the light beam and molecular motion in the medium or sample, the

optical frequency changes and, fluorescence, Rayleigh, Stokes and anti-Stokes scattering are produced. Since fluorescence is harmful to Raman spectroscopy, it is suppressed. In Rayleigh scattering, there occurs no energy changes [39]. Therefore, it doesn't carry any related information about the sample. Stokes and anti-Stokes are inelastically scattered. The transition energy of the electrons is excited by the frequency of the incident light. If the energy of the incident radiation is larger than the scattered radiation, it is named as the Stokes line. Otherwise, it is called the anti-Stokes line. The wavenumbers of the Stokes and anti-Stokes lines can be directly measured by the vibrational energies the molecules. Since the majority of the molecules are in the low vibrational energy levels, Stokes scattering is more remarkable in experiments (Figure 6) [40,41].

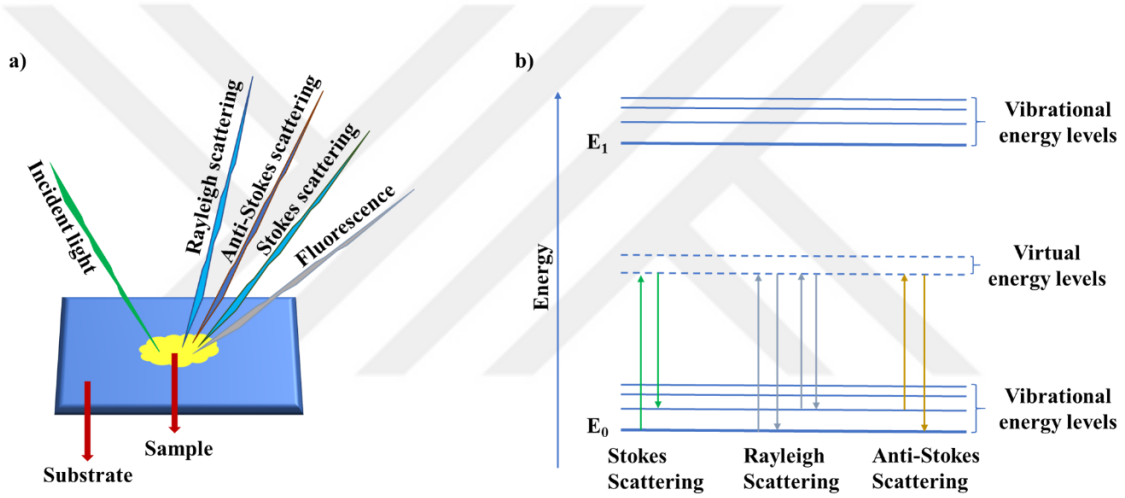

Figure 1.7. *The illustration of a) the incident light and scattering of the light on a sample and b) energy transitions involved in Raman scattering*

It is important for materials to be characterized for identifying and exploring their structures. For this purpose, Raman spectroscopy is a substantial, on-invasive and non-destructive tool for the characterization of the 2D materials. It doesn't require sample preparation and is an appropriate tool for solid-state, film samples, aqueous conditions, and gas phase [41]. Beside characterizing the structural properties, it also helps to detect the:

- layer thickness,
- band structure,
- strain effect,
- doping type, concentration,

- electron-phonon coupling,
- interlayer coupling,

of the 2D materials [40]. For example, the full width half maximum (FWHM) of Raman spectra gives information about the crystalline quality. The information of the layer number, uniformity, crystal structure and grain boundary of 2D TMDC materials can be obtained by the help of the low frequency Raman modes [40,42,43].

1.2.3. Fourier transform infrared spectroscopy (FTIR)

Infrared spectroscopy analysis is made through the interaction of the incident light with the molecules. The electromagnetic radiation interacted with a sample can be absorbed, transmitted, reflected, or scattered which gives important information related to molecular structure and the energy level transition of the sample [44].

An infrared spectrum is an individual for a sample. It represents a fingerprint of a sample with absorption peaks which conforms with the vibrational frequencies between the bonds of the atoms or molecules composing the material. Since each material has its own combination of atoms, infrared spectroscopy makes qualitative analysis for the identification of a material [45].

FTIR is a non-destructive, sensitive, fast, reliable analysis technique and precise measurement method which doesn't need to be calibrated externally. It is mechanically user-friendly and has a great optical output [45].

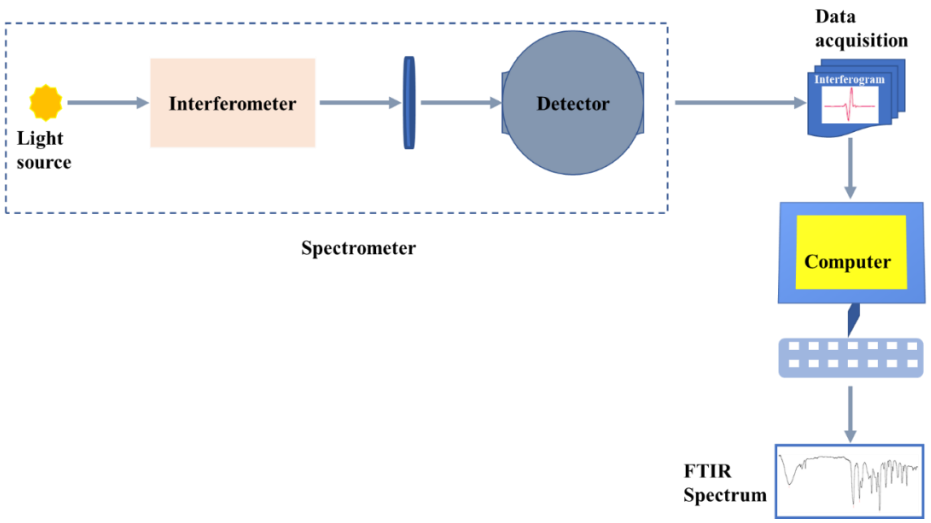

Figure 1.8. *The schematic illustration of the FTIR spectrometer*

The steps for recording an FTIR spectrum are:

1. to produce an interferogram with and without a sample in the beam
2. to transform these interferogram into the spectra of the source with sample absorption and without sample absorption.
3. the ratio of the former to the latter is the IR transmission of the spectrum of the sample.

In the case of FTIR spectroscopy, the sample is generally placed between the interferometer and the detector (Figure 7) [46].

1.2.4. Atomic force microscopy (AFM)

AFM is an effective technique which is benefited to map the topography and study the material properties on a nanoscale. AFM has a probing tip at the one end of the cantilever, which is spring-like, interacting with the sample. AFM can obtain images with atomic resolution of 10^{-10} m or one tenth of nanometer. When the tip is brought within the range of the atomic separation between the tip and sample, interatomic potentials are developed between the atoms of the tip and surface of the sample. When the tip moves on the surface, the interatomic potentials force the cantilever to bounce up and down with the changes in contours of the surface. Thus, the topography of the sample surface can be mapped out by measuring the deflection of the cantilever [47,48].

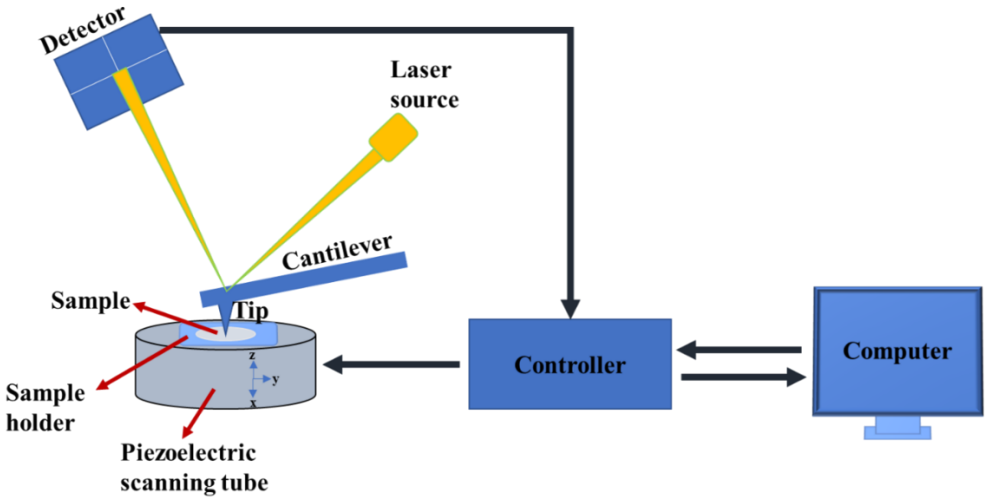

Figure 1.9. *The schematic illustration of the working principle of AFM*

Beyond topography and local force control, advanced AFM modes are also benefited to capture maps of modulus, adhesion, deformation, electrochemistry, conductivity, etc. Along with, AFM works not only under ambient conditions but also in controlled environments such as liquids, varied temperature, vacuum [49]. AFM operates in two general modes [50]:

- the static mode,
  - the contact mode (< 0.5 nm probe-surface separation)
- the dynamic mode,
  - the non-contact mode (0.5-2 nm probe-surface separation)
  - the tapping mode (0.1-10 nm probe-surface separation).

Table 1.1. *Advantages and disadvantages of the AFM modes [50]*

	Advantages	**Disadvantages**
Contact mode	✓ fast scan, ✓ good for rough samples, ✓ used in friction analysis.	✓ damage/deform soft samples.
Tapping mode	✓ high resolution of samples, ✓ good for biological samples.	✓ need slow scan, ✓ challenging to image in liquids.
Non-contact mode	✓ extended probe lifetime, ✓ very low force exerted on the sample.	✓ lower resolution, ✓ need ultra-high vacuum.

1.2.5. Four-point probe method

For the indications of the changes in the chemical binding nature, the electrical resistivity is one of the most sensitive ways. Generally, it is inversely proportional to the carrier density and the carrier mobility. A change in the chemical binding nature primarily causes alterations in the carrier density, and the carrier mobility is altered by structural changes [51].

In material science and semiconductor industries, four-point probe characterization technique is used to determine the electrical properties of thin and solid films because it

requires low demand on the preparation of the sample and it provides high accuracy. It is also very appropriate technique for low resistance measurements since it eliminates the effects of the contact resistance between the sample and contacts. This method can be used to specify the resistance of the specimen in both single crystal and bulk forms. In this method, through the outer contacts, the current flows and across the inner contacts, the voltage is measured [51,52].

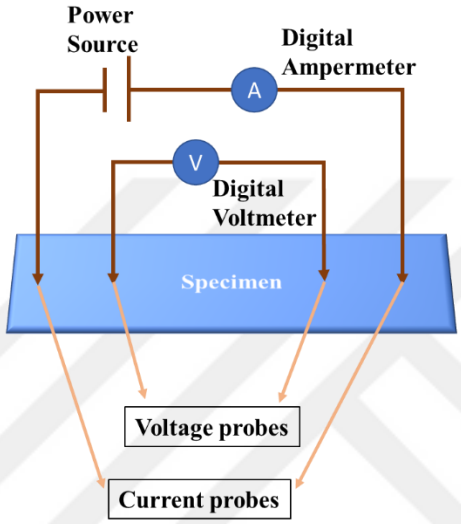

Figure 1.10. *The schematic illustration of the four-point probe method*

1.3. The State of Art of the Biosensor Applications

A biosensor can be described as a monitoring device which is capable of reading and converting a biological response into physical, chemical or electrical signals [53]. The biosensor consists of two parts: a receptor and transducer. The receptor receives the physical or chemical stimulus and afterwards it transmutes the information in the form of electrical energy [54]. On the other hand, the transducer identifies the biological interaction and convert it into measurable signal by making use of a range of physical or chemical phenomena. Shortly, the bioreceptor recognizes the target molecule (the analyte) while the transducer converts biological response into a measurable signal by devices [55]. The receptor can be an antibody, an enzyme, a nucleic acids, or a whole cell. The transducer can be a surface plasmon resonance, a field effect transistor (FET), a metal nanoparticle, an enzymatic reaction, or an electrode [56].

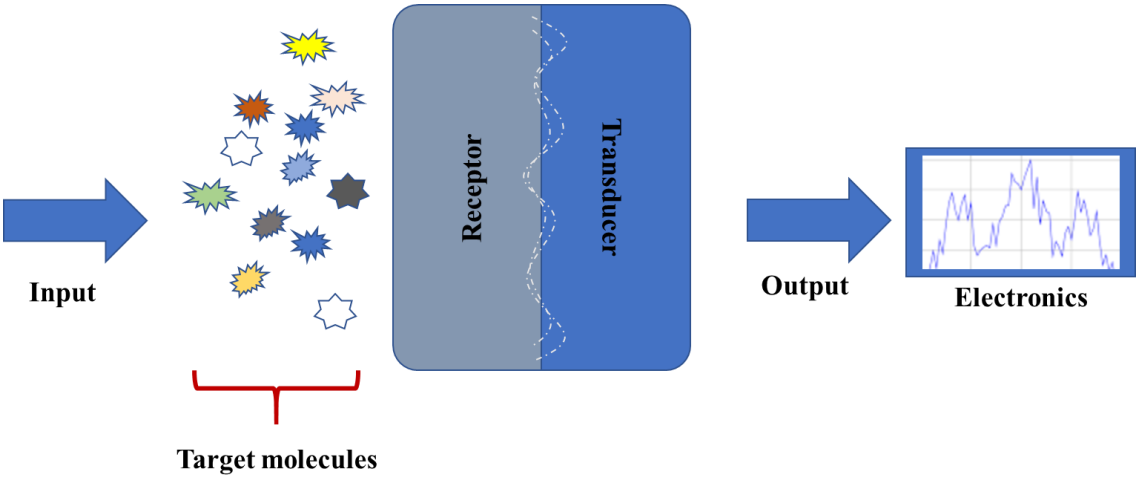

Figure 1.11. *The schematic of the components of a typical biosensor*

Owing to their outstanding outcomes, biosensors have been used in distinct scientific disciplines in a wide range. They can be benefited for an accurate and precise detection of tumors, pathogens, or other toxins in medical. They can be also used in food industry, environmental safety, military defense system. In these cases, they can be available for the use of the detection air pollution, heavy metals, gases from spoiled foods, food contamination, the presence of any harmful biological materials, and preventing the growth of bacteria. Therefore, the biosensor has to meet some substantial requirements such as high sensitivity, selectivity, portability, reproducibility, cost-effectiveness, and stability. Furthermore, it needs to operate fast and be manufactured easily [53-55].

Biosensors can be classified by utilizing various approaches [54]:

- Based on the transduction principle (electrochemical, optical, mass dependent biosensor),
- In terms of bio-element (enzyme, nucleic acid, protein, ligands biosensors),
- Depending upon the type of the analyte detection (glucose, DNA, drugs toxins).

1.3.1. Optical biosensors

The basic principle of the optical biosensors is the interaction of the light with biological molecules. This interaction provides a range of observable optical phenomena used to derive the information related to system. The interaction can result in the light absorption, scattering, change of refractive index, or emission of radiation. These

biosensors are based on the absorption, fluorescence, Raman scattering, and refractometry [55].

1.3.1.1. Absorption spectroscopy

Absorption spectroscopy is based on the light absorption by biomolecules at a certain wavelength. In this process, the photon energy is taken up by the atoms or electrons in the matter. Spectrophotometer is a quantitative device to measure the sample absorbance. To determine the substance concentration, kinetic measurements of particular biochemical reactions, and to identify some biological species. It is also a prominent tool which is used in biological experiments to detect nucleic acids and protein quantity. Nevertheless, the main limitation of all of the absorption based optical transducers is the deficiency of the variant absorption patterns from which they might be identified [55,57].

1.3.1.2. Photoluminescent biosensors

Florescent based optical transducer is one of the most commonly used technique because of its high sensitivity. Fluorescence eventuates when a fluorescent atom absorbs a photon of high energy exciting an electron into one o the many higher energy states. This brings out the fluorescent molecules to emit photons of lower energy in return for the light absorption from the external source. This radiative emission can be detected and the concentration of the fluorescent molecules can be indicated by the intensity of light. Thus, if the analyte is bound to fluorescent label, its concentration can be determined. Even though fluorescence is commonly used in biosensors, fluorescent quenching is always a problem where a fluorophore collides with another molecule resulting in return to its ground state without emitting photon.

Another powerful analytic technique widely used in biosensing is Raman spectroscopy. Raman scattering which is the inelastic scattering of photons that interacts with vibrating molecules in the sample is an underlying phenomenon of this technique. The energy of the vibrations of the molecules is transferred to or received by the photons. Thus, the energy change is corresponding to the vibrational energy of the molecules in the matter. Although the Raman technique is a highly efficient way to be used for small chemical compounds, depending on the large number of possible vibrational states, large macromolecules can end in very complex Raman spectra [55,58].

1.3.2. Potentiometric biosensors

These biosensors are electrochemical biosensors which operates at a constant current. Potentiometry gives information regarding the ionic activity in an electrochemical reaction. These biosensors are used to measure the charge density variations on the electrode surface following a catalytic reaction or selective binding of a molecule as a surface modification. Ph electrode, light addressable potentiometric sensor, ion-sensitive field effect transistor (ISFET), chemically modified FET, and enzyme immobilized ISFET can be given as examples for the applications of these biosensors [53].

1.3.2.1. Enzyme immobilized ISFET

In ion-sensitive field effect transistors (ISFETs), the gate metal electrode of the metal-oxide-semiconductor FET (MOSFET) is replaced by an electrolyte solution. This electrolyte solution contacts with the reference electrode. In ISFET devices, the source-drain current flows from the source to drain through the channel. The source-drain current is affected by the interface potential at the oxide-aqueous solution [53].

ISFET is a robust platform to advance biosensors. Gate surface of a FET is attached with enzymes or antibodies using several methods. Here, the immobilization of the enzyme on the surface of Gate is very important. These sensors are developed on the change of gate material, composition of the enzyme membrane, or immobilization method. Many analytes such as glucose, ascorbic acid, lactate, creatinine can be detected by the usage of these biosensors [53,56].

1.3.3. Enzyme immobilization

Immobilization of enzymes or cells corresponds to the technique of confining or anchoring the enzymes or cells in or an inert support for the functional reusage or stability. The immobilization of the enzymes provides some advantages:

- causing increasement the stability and efficiency of the enzymes,
- reusage of the enzymes,
- controllability over the function of the immobilized enzymes,
- using free enzymes for reaction products,

- suitable for industrial and medical usage.
- less effluent disposal problems.

On the other hand, the enzyme immobilization also causes some drawbacks such as reduction of the biological activity of the enzymes and expensive immobilization processes. Adsorption, entrapment, covalent binding, encapsulation, and cross-linking are mostly used immobilization techniques [53].

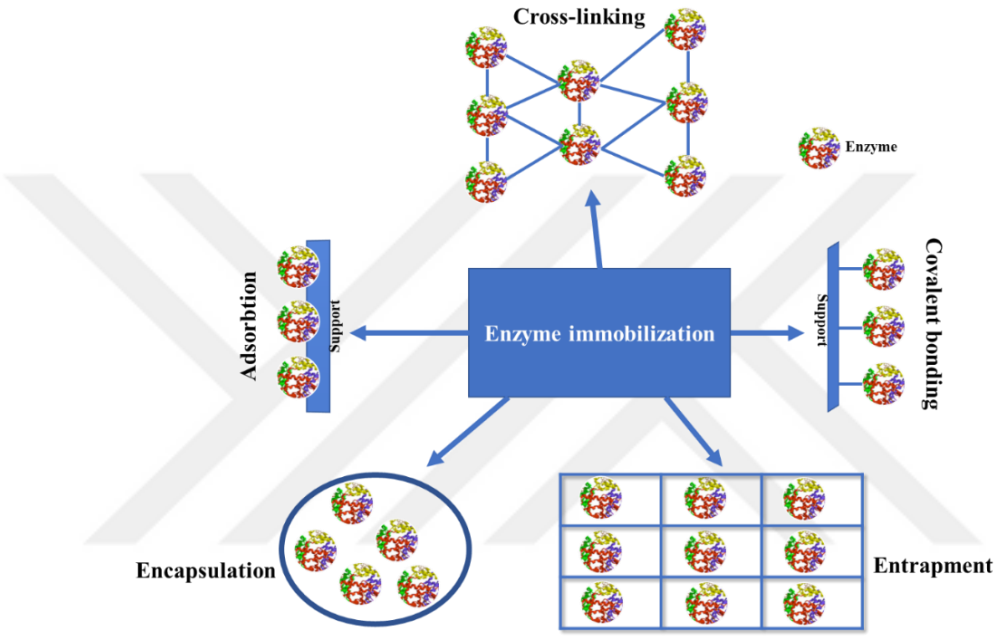

Figure 1.12. *The schematic illustration of the Enzyme immobilization techniques*

The immobilization methods are briefly defined as [53]:

Adsorption method: There is physical binding between the enzymes or cells and the surface of an inert support.

Entrapment method: Enzymes are physically entrapped inside a polymer or a gel matrix.

Encapsulation method: It is a kind of entrapment which liquid or suspension is comprised in a semipermeable membrane.

Covalent-binding method: There exists a covalent bond between the chemical group of enzymes and the support matrix.

Cross-linking method: The immobilization is made by the formation of cross-links between enzyme molecules.

2. EXPERIMENTS AND DISCUSSIONS

In this thesis, CVD and ALD techniques are utilized for the growth of 2D materials. Different types of 2D TMDC materials are successfully grown by the help of different growth approaches. Most of the growth and characterization tools are facilitated in our research laboratory.

2.1. CVD Growth Optimization Studies

To be able to grow 2D materials, some precursors or sources are needed depending on the type of the material which will be grown or the deposition method that will be used. The Mo source can be a powder [59], foil [60] or thin film [61]. In this thesis, both powders and thin films are used as Mo sources. Also, to provide controllability, reproducibility and high-quality for the materials, different type of configurations, sources, gases can be appealed.

Four different approaches are used in this work, which are: face-up and face-down growth, ALD assisted growth, glass assisted growth and on glass growth. Except on-glass-growth, 2D materials are attempted to be grown on SiO_2/Si (300 nm oxidized layer of SiO_2 on Si) substrate.

After completing the growth processes of the materials, optic microscopy (bright and dark field) images, Raman spectroscopy (WITec Alpha300-R,) atomic force microscopy (ez-AFM, Nanomagnetic Instruments), FTIR (Shimadzu AIM-8800) tools are used to characterize the grown materials.

2.1.1. Face-down growth method

In this section, there are two ways for SiO_2/Si substrates to be used. In the face-down method, SiO_2/Si substrate is positioned as oxidized SiO_2 surface is looking/facing down, and Si surface is looking/facing up (Figure 2.1).

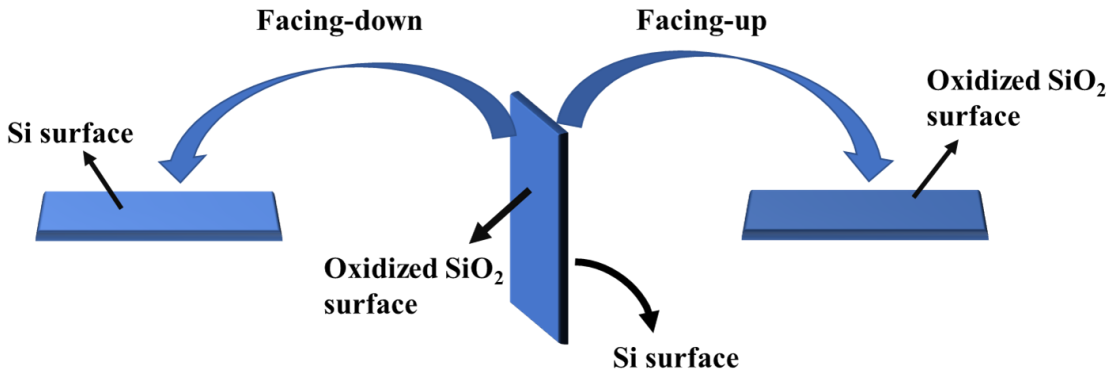

Figure 2.1. *The schematic of face-up and face-down position of the SiO_2/Si substrate*

2D MoS_2 growth has begun with using face-down methodology. 2 cm x 3 cm cleaved SiO2/Si is replaced on the top of MoO_3 powder, which is used as molybdenum (Mo) precursor, in a face-down position. In all of these experiments, SiO_2/Si substrates are cleaned by some chemicals before being used in the growth. They are vibrated in acetone, iso-propanol, deionized (DI) water for 5 minutes by ultrasonic vibration tool, respectively. Sulfur (S) powder is used as sulfur precursor. Nitrogen (N_2) gas is used a carrier gas with the assistance of the low rate of hydrogen (H_2) gas. This experiments are operated under environmental conditions. The two-temperature zones of the furnace are set to be at 690 ^oC. The growth parameters for this experiment are: 2 mg MoO_3 powder, 150 mg S powder, 95 sccm N_2, and 5 sccm H_2. At the end of the experiment, the furnace is left to cool down naturally.

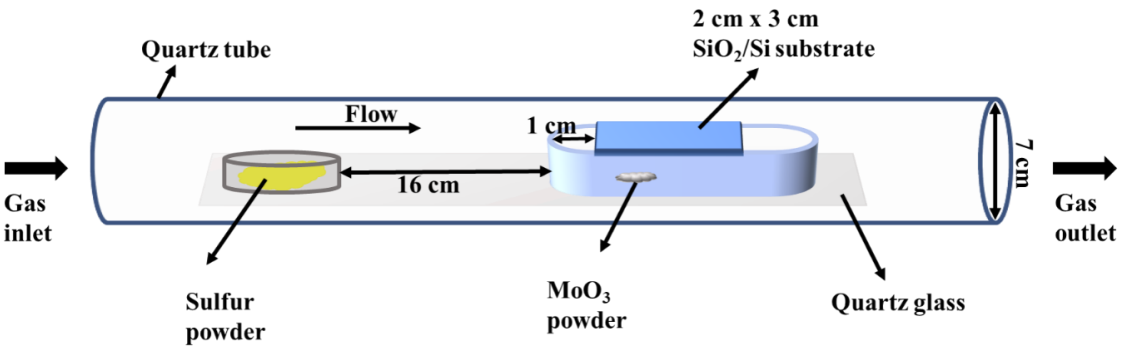

Figure 2.2. *The schematic illustration of the growth configuration of the 2D MoS_2 material*

Under optical microscopy, it is observed that the grown materials are triangular shaped MoS_2 flakes with homogenous and large surfaces. When the Raman spectra

measurements of these MoS_2 flakes are taken, two characteristic E^1_{2g} and A_{1g} peaks of the MoS_2 material are observed. E^1_{2g} represents the in-plane mode which is resulted from the opposite vibration of two S atoms in regard to the Mo atom. A_{1g} indicates out-plane mode which is caused by the vibration between only S atoms in opposite directions[62]. The changes in the frequency of these modes are corelated to the number of the layer of MoS_2 material [63]. For monolayer MoS_2 structures, the difference between these two modes is expected to be less than 22 cm^{-1} [63,64]. Here the measurements are performed with a laser source that has a wavelength of 532 nm (2.3 eV), and spot size approximately 0.8 μm. The laser power is adjusted to be 0.5 mW to prevent damaging the MoS_2 flakes. In our results Raman spectra are observed at 383.91 cm^{-1} for E^1_{2g} mode and at 405.43 cm^{-1} for A_{1g} mode. The difference between these peaks is measured as 21.52 cm^{-1}, which indicates that the grown MoS_2 flakes are monolayer. When it comes to observe of PL spectra of monolayer MoS_2 flakes, PL peaks are expected to be approximately at the points of 1.8 eV, 1.84 eV, 2 eV for Trion, A-exciton, and B-exciton, respectively [12,65,66]. In our measurements, PL peaks are observed at the points of 633.91 nm (1.96 eV), 678.76 nm (1.83 eV), 684.45 nm (1.81 eV) for B-exciton, A-exciton and Trion peaks, respectively. The measurement results are given in the following Figure 2.3.

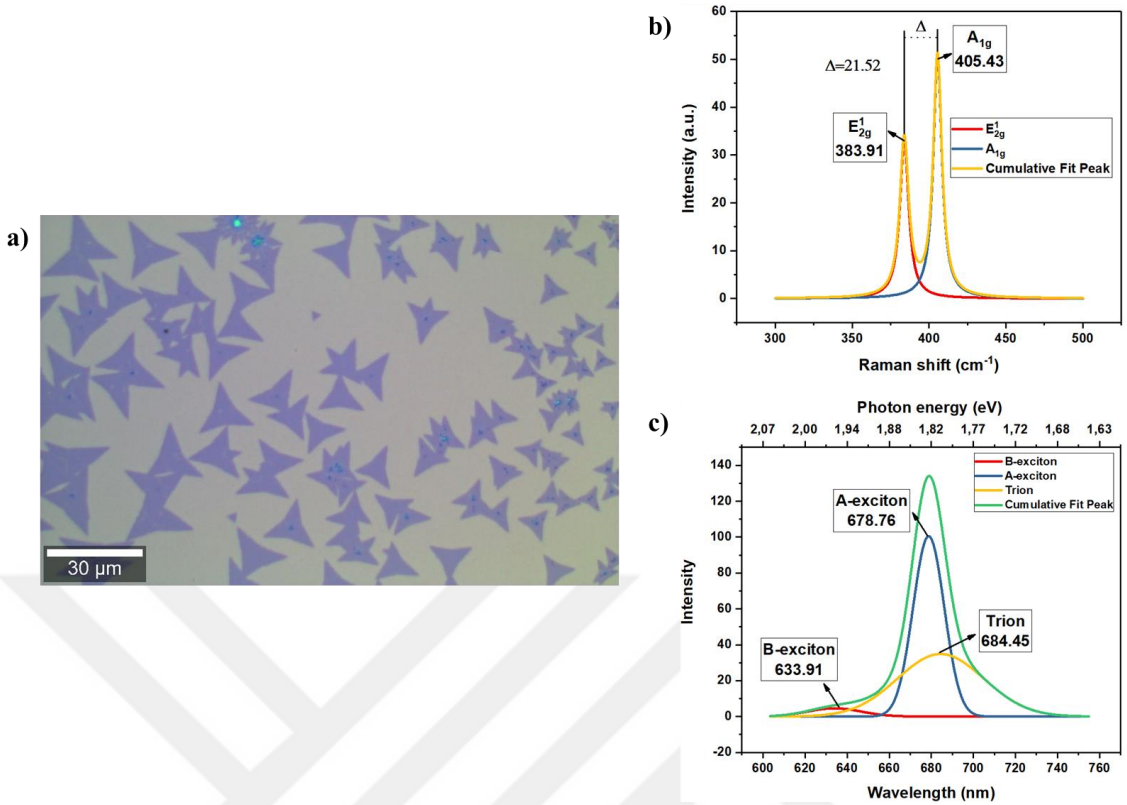

Figure 2.3. *a) Optical Microscopy image of MoS_2 flakes grown on the face-down substrate. b) Raman and c) PL spectrum of grown MoS_2 flakes*

2.1.2. ALD-assisted growth method

Even though growing monolayer MoS_2 materials by the help of this method is successfully achieved, it is lack of the flake size controllability. By changing the Mo precursor from MoO_3 powder to MoO_3 thin film, the flake size controllability is tried to be overcome. MoO_3 thin films are deposited on the SiO_2/Si substrates at different thicknesses by the ALD technique. Here, ALD is very helpful tool for depositing thin film with a certain thickness. By taking advantage of the controllability of the thin film thickness, the Mo precursor, the flake sizes of the grown MoS_2 material is taken under control.

It is believed that the growth cycles of the thin film deposition help to determine the thickness. As the growth cycle increases, the thickness of the thin film also increases. Therefore, the deposition of MoO_3 thin film is started with 600 cycle and ended in 1 cycle. In deposition process, firstly $MoCl_6$ is used as precursor. However, the bonds between Mo and Cl atoms are too strong, they can't be broken by our sources which are available in our laboratory. So, the MoO_3 film deposition couldn't be succeeded through the usage

of $MoCl_6$ precursor. Thus, $Mo(CO)_6$ is used as another Mo precursor in ALD process. At the end of some experiments, it is seen that $Mo(CO)_6$ precursor is more appropriate to be used in our system for MoO_3 thin film deposition. Here, to break the bonds between Mo and carboxyl group, oxygen plasma is utilized. This is resulted it in achieving MoO_3 thin film deposition at lower temperature. The deposition of the MoO_3 thin film is started with pulsing $Mo(CO)_6$ precursor during 3 seconds into deposition chamber which is set at 160 ^oC. Then, it is pulsed out of the chamber for 4 seconds. Followingly, O_2 plasma is exposed into the chamber for 3 seconds. Finally, after exposure, excess chemicals and by products are purged out of the chamber by the help of the N_2 carrier gas for 3 seconds. This process states only one cycle of the deposition.

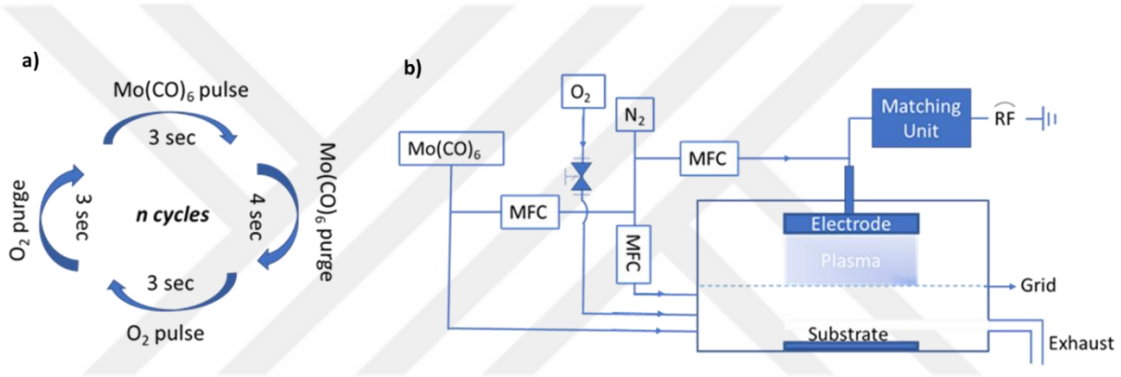

Figure 2.4. *The schematic configuration of a) cyclic deposition of the MoO_3 thin films b) the ALD system including the precursors or sources which are used to deposit MoO_3 thin films*

Deposited MoO_3 thin films are characterized by Raman spectroscopy, FTIR and AFM tools. It is seen that the as-grown MoO_3 thin films have no Raman spectra because their structure is amorphous. To make sure that the grown materials are MoO_3 thin films, they are annealed at different temperatures. By doing so, since the annealing brings out some phase changes in the structure of the MoO_3 material depending on the temperature, the Raman spectra can be observable. The MoO_3 thin films are firstly annealed at 400 ^oC and 600 ^oC which are corresponding to β and α phases, respectively [67]. Afterwards, when they are characterized by Raman spectroscopy, it is founded that the grown material is MoO_3 because the Raman spectra are matching with the characteristic Raman peaks of β-phase MoO_3 are: 773 cm^{-1}, 845 cm^{-1}, and 904 cm^{-1} [67]. The Raman peaks of -phase MoO_3 are: 275 cm^{-1}, 330 cm^{-1}, 369 cm^{-1}, 657 cm^{-1}, 811 cm^{-1}, and 987 cm^{-1} [68]. Along with these spectra which are taken by the laser source in the visible range, it is made use of FTIR to observe the peaks in the infrared range (IR). It is approved that the grown

material is MoO_3 by the characteristic peaks which are observed in the IR range by FTIR. The FTIR results are obtained as the followings: 814,55 cm^{-1} and 1004,23 cm^{-1} for α-phase; and 779,41 cm^{-1}, 880,47 cm^{-1} and 961,01 cm^{-1} for β-phase of MoO_3 thin films deposited by ALD system. It is seen that the FTIR results are relatively matched with the peaks in the literature, which are: 1125 cm^{-1}, 988 cm^{-1}, 884 cm^{-1}, 618 cm^{-1}, and 460 cm^{-1} [68].

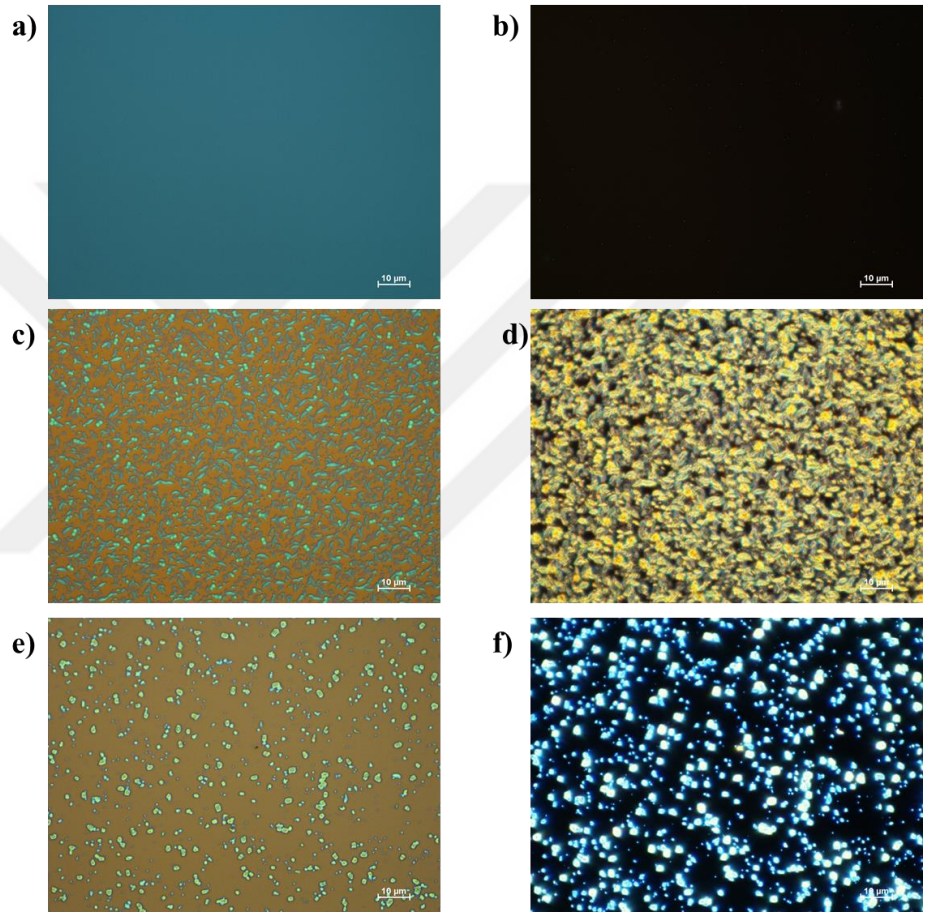

Figure 2.5. *The optical images of ALD deposited MoO_3 thin film with 150 cycles. a) bright field and b) dark field images of as-deposited film; c) bright field and d) dark field images of the MoO_3 film annealed at 400 ^oC; e) bright field and f) dark field images of the MoO_3 film annealed at 600 ^oC*

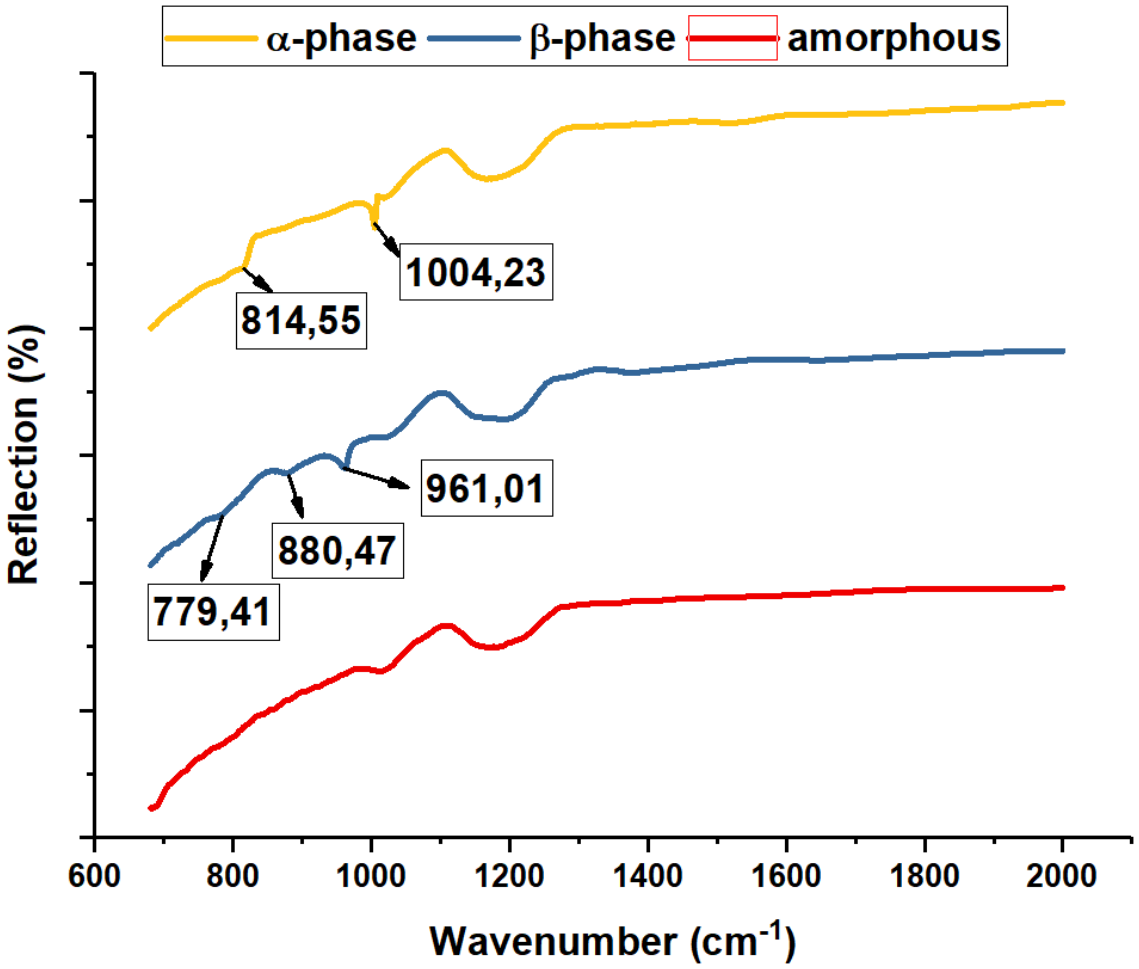

Figure 2.6. *FTIR measurements of the different phases of MoO_3 thin films: amorphous: as-deposited MoO_3 thin films, β-phase: annealed MoO_3 thin films at 400 °C; and α-phase: annealed MoO_3 thin films at 600 °C*

After completing the deposition of the MoO_3 thin films, the deposited MoO_3 thin films are used in CVD system for the MoS_2 growth. Here, MoO_3 thin films deposited at different cycles, referring to different thicknesses, are included into the CVD system to observe the effect of the usage of the thin films as Mo precursor. MoO_3 thin film coated SiO_2/Si substrate (1,5 cm x 1 cm) is positioned as face-up in the growth configuration in CVD system; and clean SiO_2/Si substrates (2 cm x 3 cm) are placed on the top of it in face-down position. Thus, both face-down and face-up growth approaches are benefited with the assistance of ALD technique. This growth process is also performed under ambient conditions. The growth temperature and the quantities of the sulfur and carrier gases are kept the same as previous experiment. At the end of the experiments, it is observed that the alterations in the cycles of the MoO_3 thin films cause the changes in the size of the MoS_2 flakes.

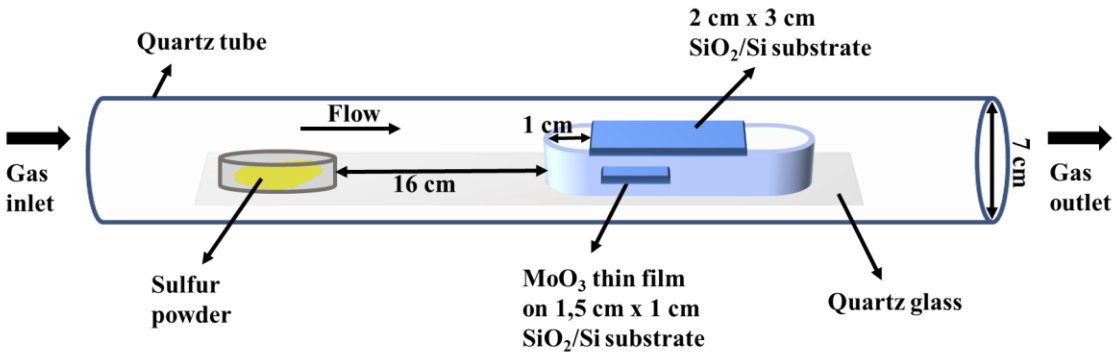

Figure 2.7. *The drawing of the CVD system which includes MoO_3 thin films as Mo precursor*

The grown MoS_2 materials are firstly observed under optical microscopy. It is seen that the thickness alteration in MoO_3 thin films cause different formations in MoS_2 material. As the thickness of the MoO_3 thin films decreases, the flake sizes of the grown MoS_2 structures get smaller. Moreover, the thickness of the small flakes also diminishes. On the contrary, when the number of cycles of the deposition of the MoO_3 thin films rises, it is seen that the flake size increases and the large monolayer MoS_2 flakes start to form. The higher number of the deposition cycles of the MoO_3 thin films cause the formation of small MoS_2 flakes on the surface of large MoS_2 flakes. This creates problems related to the formations of the homogenous monolayer MoS_2 flakes for electronic and optical device applications. According to optimized experimental results, the large MoS_2 flakes can be grown by 150 cycles with homogenous surface. As the thickness of the MoO_3 thin films increases (>150 cycles), it is observed that the small MoS_2 flakes starts to form on the monolayer flake surface. Also, multilayer MoS_2 flake formations can be observed. Most probably, this is because the MoO_3 source on the surface of the small substrate is uniformly distributed. The more thickness causes more aggregation on the upper large substrate because of the raising temperature. This brings out the MoS_2 flakes to become thicker since the growth occurs horizontally unlike laterally.

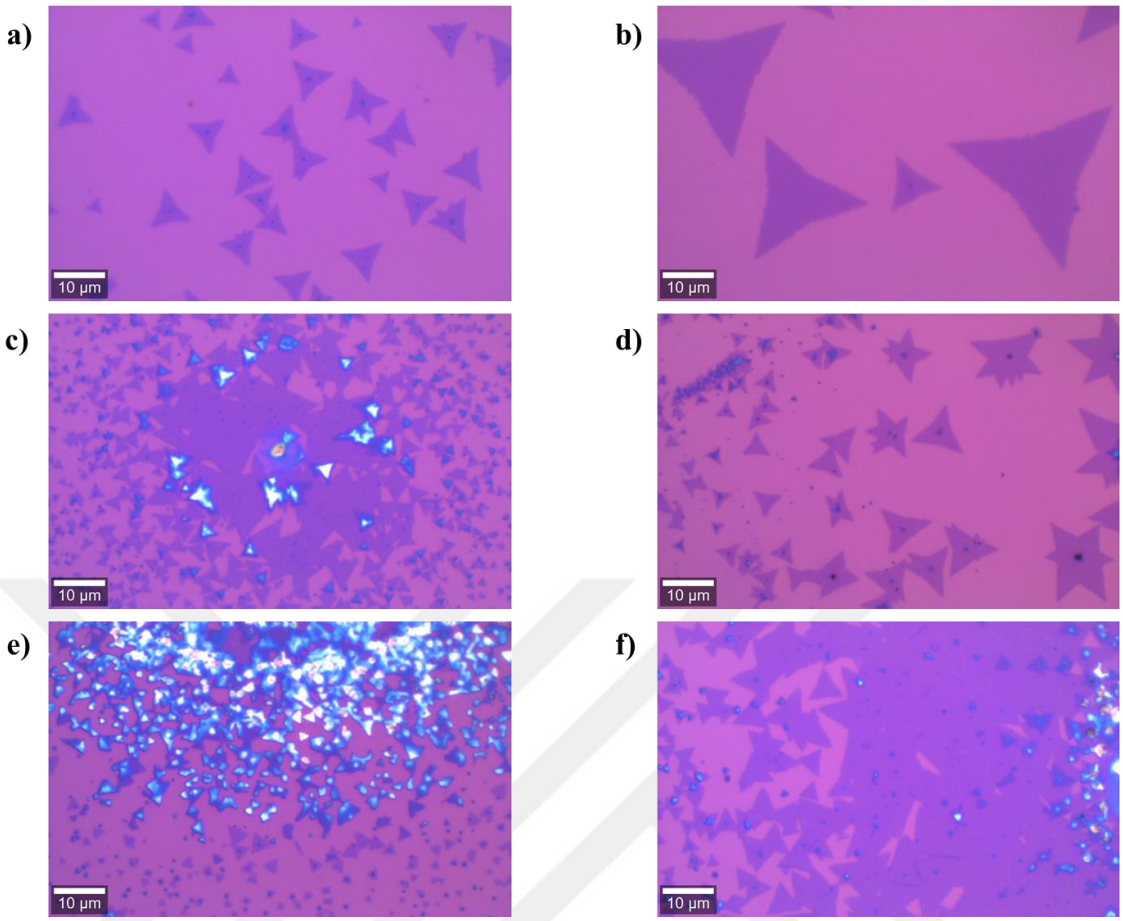

Figure 2.8. *The optical images of MoS_2 flakes grown by CVD method with different cycles; a) 150 cycles, c) 300 cycles, e) 600 cycles on bottom substrate and b) 150 cycles, d) 300 cycles, f) 600 cycles on upper substrate*

Also, with very small number of cycles, very small monolayer MoS_2 flakes formation can be obtained. Depending on the inadequate source of volatized MoO_3 provided to the upper substrate, the MoS_2 flakes remain small; and the formation occurs horizontally as the thickness of MoO_3 thin films increases. These results are obtained by Raman spectroscopy and AFM measurements. This growth method which helps to grow different physical properties of the MoS_2 flakes such as small, large and non-homogenous can be benefited according to the purpose of the application field or usage.

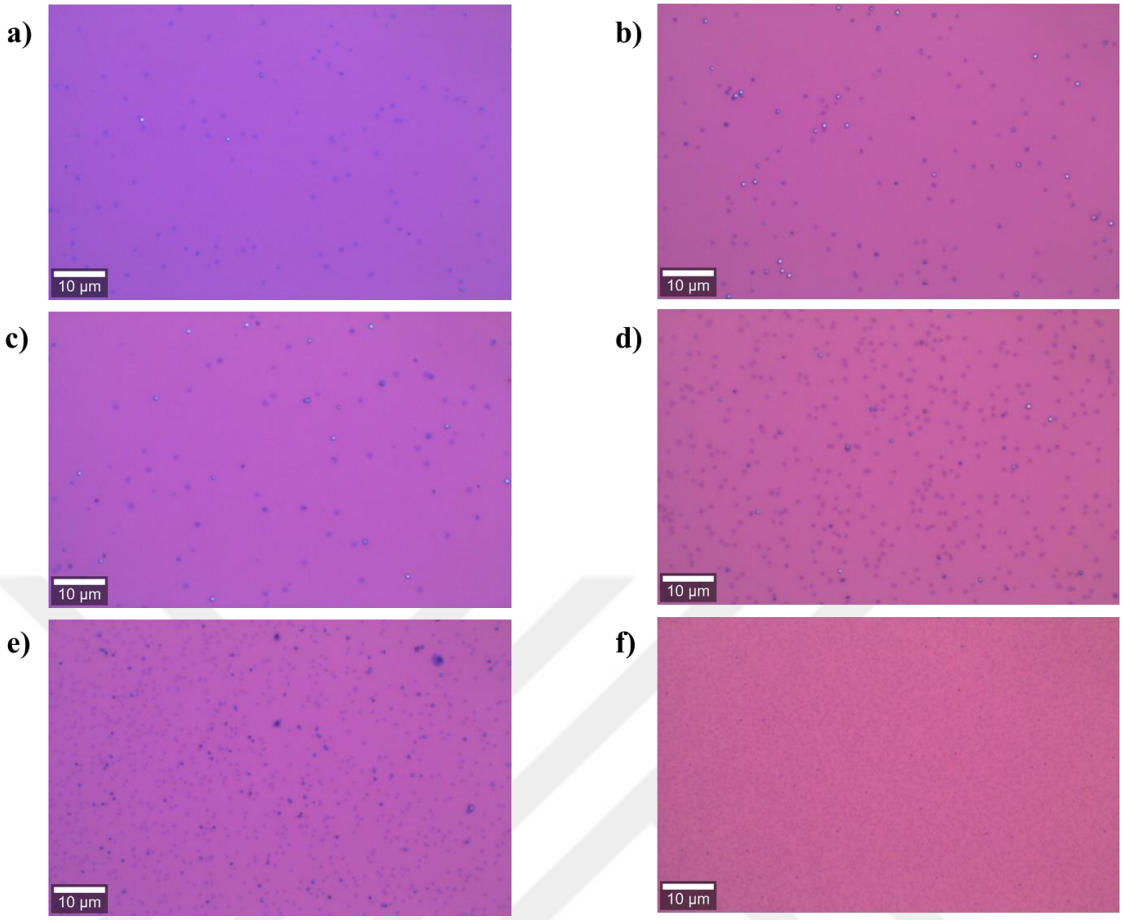

Figure 2.9. *The optical images of very small MoS_2 flakes grown by CVD method with different cycles; a) 1 cycle, c) 10 cycles, e) 25 cycles on bottom substrate and b) 1 cycle, d) 10 cycles, f) 25 cycles on upper substrate*

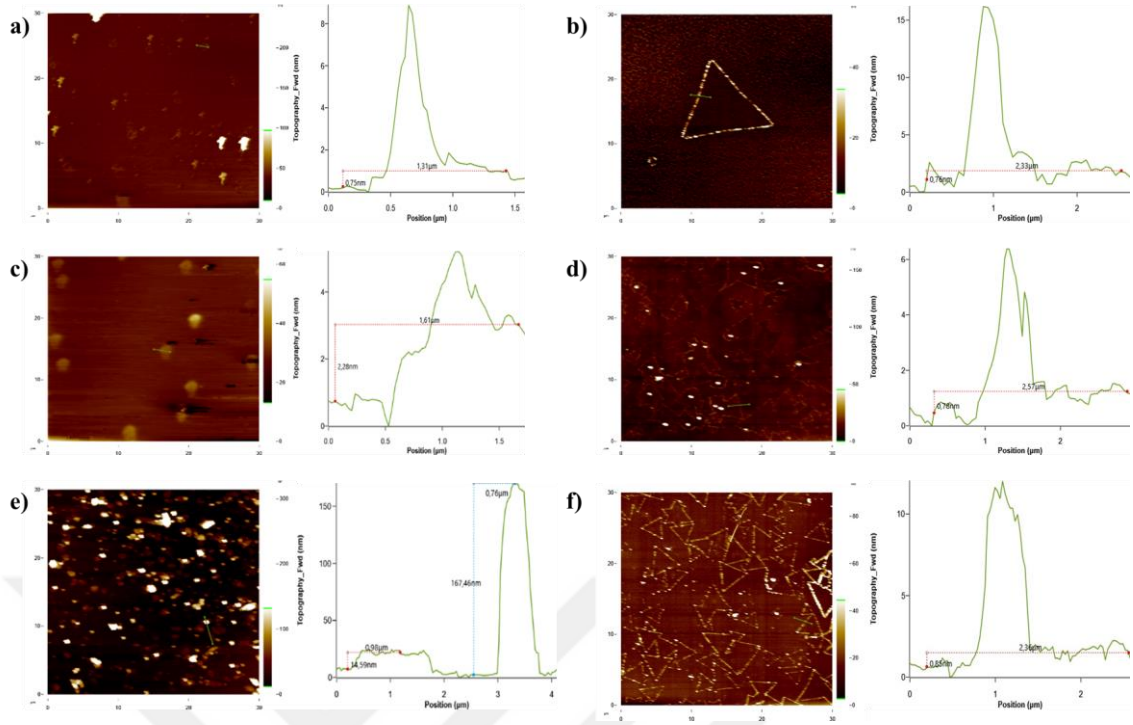

Figure 2.10. *The AFM topography images and thickness measurements of MoS_2 flakes in different cycles: a) 1 cycle, c) 10 cycles, e) 25 cycles which are lower cycles; and b) 150 cycles, d) 300 cycles, and f) 600 cycles*

2.1.3. Glass-assisted growth method

Despite MoS_2 growth with ALD assistance is a good way to obtain monolayer flakes, using a piece of a glass (2 cm x 2 cm) in the experiments has shown that growing three different TMDC materials is more possible that way. WS_2, $MoSe_2$, and MoS_2 materials are successfully grown by using glass in the experiments. This growth method also solves the problems of controllability, reproducibility and consistency for obtaining 2D TMDC materials at the end of the CVD experiments. This experiments are carried out under a controllable inner pressure of the quartz tube in the furnace. The importance of this growth approach is that the three different TMDC materials are attempted to be grown by using the almost same configurations and conditions. For example, the pressure is kept higher than atmosphere pressure for all the materials growth. Also, in these experiments, powder precursors are used instead of thin films.

Table 2.1. *The growth parameters of the TMDC materials*

Parameters/ Materials	S/Se powder	MoO_3/WO_3 powder	N_2 flow (sccm)	H_2 flow (sccm)	Growth temperature	Growth pressure (Torr)	Growth duration
MoS_2	150 mg S	4 mg MoO_3	95	5	700 ºC	740	6 min.s
$MoSe_2$	150 mg Se	4 mg MoO_3	95	5	900 ºC	730	6 min.s
WS_2	150 mg S	4 mg WO_3	95	5	900 ºC	740	3 min.s

The growth parameters and configurations are given and shown in the Table 2.1 and Figure 2.5, respectively.

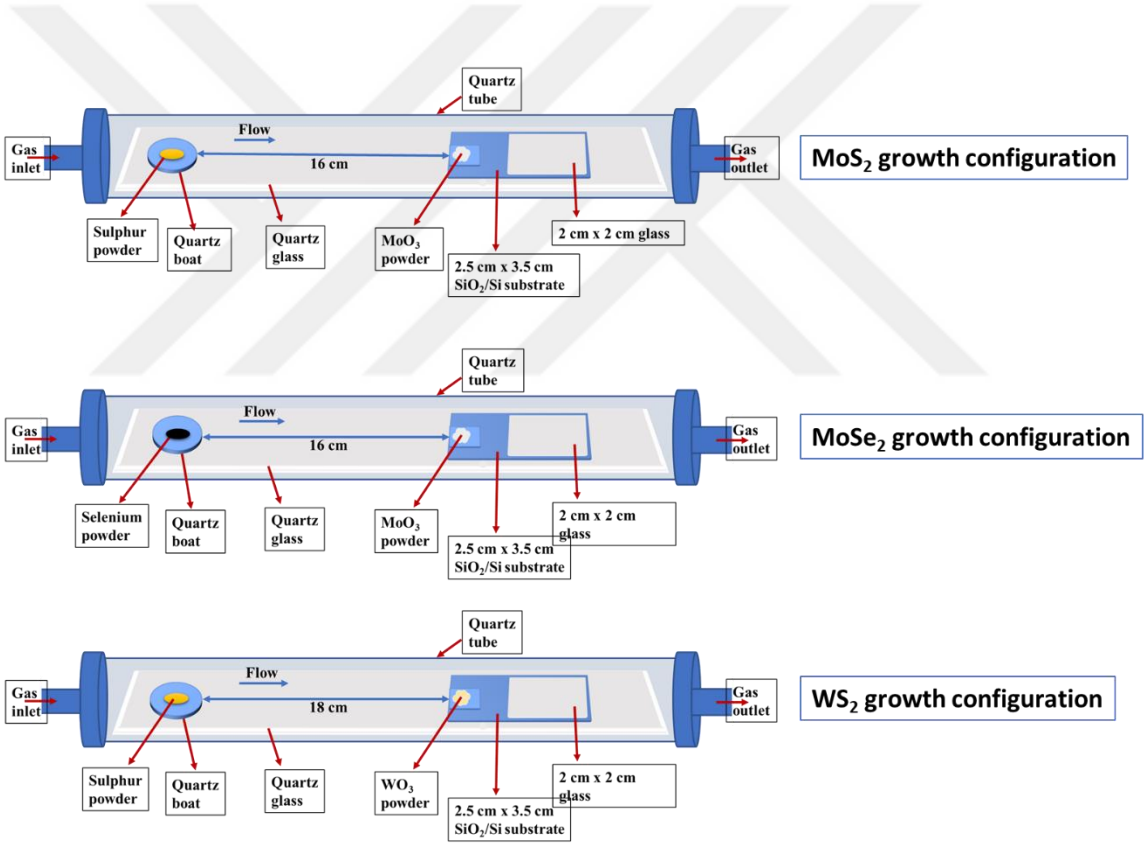

Figure 2.11. *The schematic of the growth configuration of the different TMDC materials used in CVD system*

At the end of this growth approach for different three 2D materials, it is observed that the grown materials have a large surface area. It is also seen that the formation of the grown materials may differ. That's, some of the grown materials may have non-homogeneities on the surface of the flakes. Furthermore, the growth area of the materials

changes according to their vaporization rate and volatility. For example, for MoS_2 and $MoSe_2$ materials, the surface of the large substrate is covered continuously. However, for WS_2, the coverage of the surface of the large substrate is quite a little because of its low volatility. Also, on the surface of the large substrate, it is noted that the flake sizes of the grown MoS_2 and $MoSe_2$ materials increases towards the dashed arrow shown in the Figure 2.9. For WS_2 material, the growth occurs on the small substrate on which the WO_3 powder is put. The WS_2 film is grown around the powder. As it is getting closer to the edges of the substrate, the WS_2 flake formation arises.

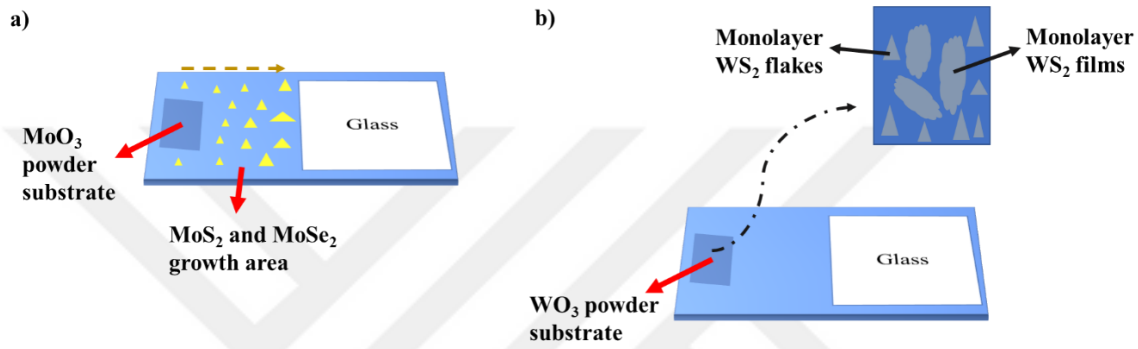

Figure 2.12. *The growth area of a) MoS_2 and $MoSe_2$ and b) WS_2 materials*

After examining the grown sample under optical microscopy, Raman and PL measurements are taken.

2.1.4. Direct growth on glass

The reason to use this growth method is because harvesting MoS_2 materials from glass surface by the help of DI water becomes easier in contrast to SiO_2/Si surface. Here, this configuration provides many samples on which 2D MoS_2 material is grown. Therefore, it can be made use of this method to harvest grown 2D materials from the surface of the glasses for biosensor applications.

In this method, some growth parameters have been changed. The amount of S is made 300 mg and the amount of MoO_3 powder is 0.5 mg. The flow rate of N_2 and H_2 gases are 180 and 20 sccm, respectively. The growth temperature is set to be at 750 ^oC and the pressure is 750 Torr. At the end of this configuration, it is observed that MoS_2 is grown on the surfaces of the glasses. And the size of the grown of 2D MoS_2 materials are

decreasing as the formation of MoS_2 is decreasing towards the last piece of the sample, which is indicated by the dashed blue line in the Figure 2.6.

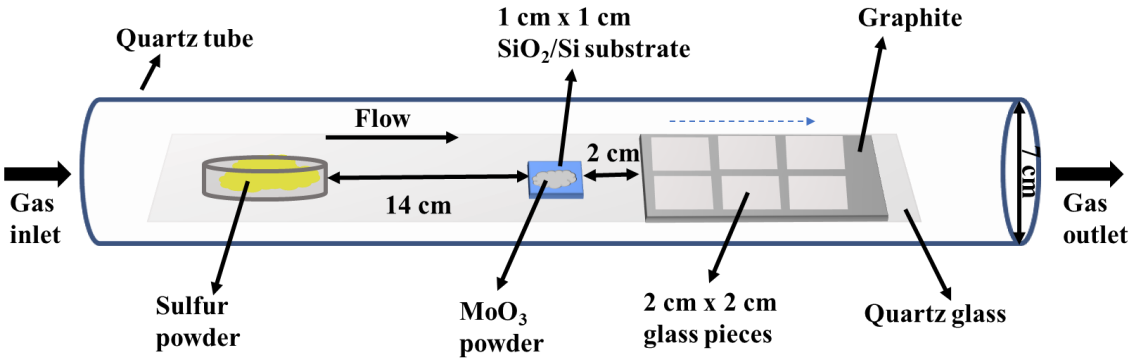

Figure 2.13. *The growth configuration of MoS_2 material on a piece of glass by CVD method*

After completing growth experiments on glass substrate, MoS_2 flakes are firstly transferred on the SiO_2/Si substrate. This method, growing MoS_2 flakes on the glass, eases the way for harvesting the flakes from the surface of the glass as it is experimented in the future works. To make sure that the grown MoS_2 material on glass is monolayer, Raman spectroscopy measurements are taken as grown on glass. These flakes are used for both preparing the solution of the enzyme-MoS_2 structure and FET device fabrication which are explained in the next sections.

According to the Raman spectroscopy measurements, it is seen that the grown MoS_2 flakes on glass substrate are monolayer, which is concluded regarding to the difference between the Raman peaks which is equal to 19,11 cm^{-1}. They have also a large surface area. The length of the one edge of the triangular MoS_2 flake is measured as 78,3 μm. It is also seen that the grown MoS_2 flakes have a high PL intensity.

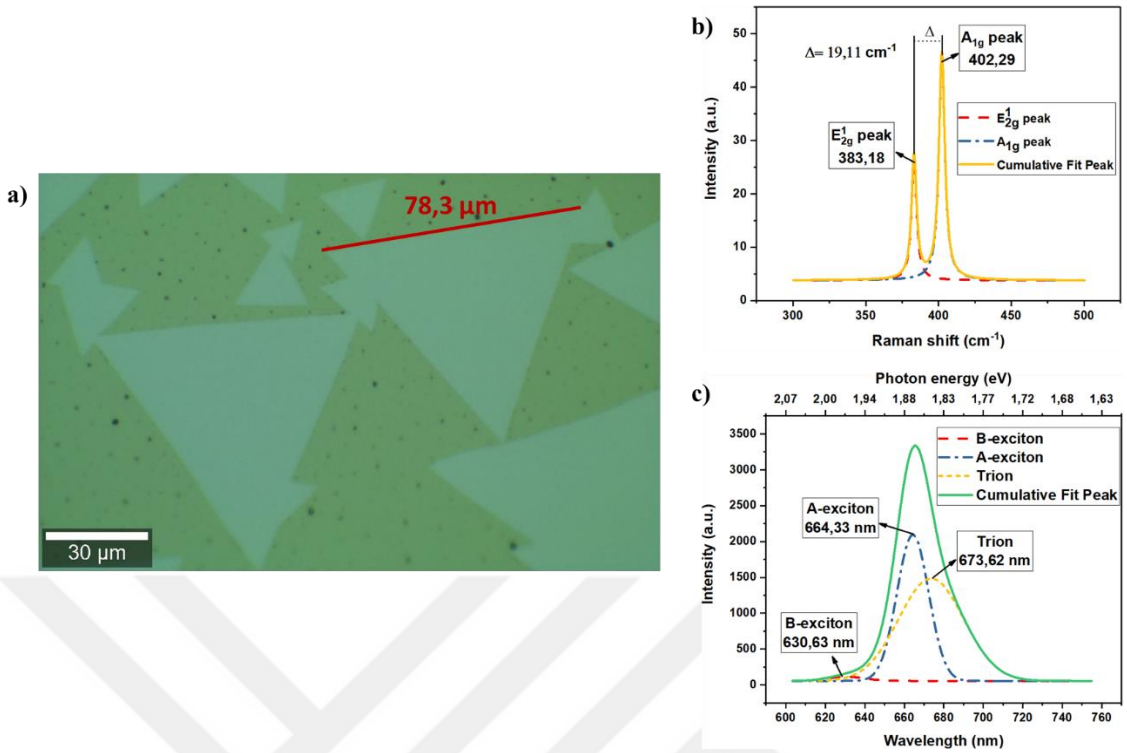

Figure 2.14. *a) The optical image and b) Raman and c) PL spectrum of the CVD grown MoS_2 flakes on glass substrate*

2.2. Sensing Application of Monolayer MoS_2 on HRP Enzyme

In these experiments, three different approaches are investigated for the detection of the enzyme. The first approach is using Raman spectroscopy tool to observe the changes in Raman and PL spectra. Secondly, the spectrophotometer tool is used to observe the activity of the enzymes which are in the interaction with the monolayer MoS_2 flakes. As the last approach, FET device is fabricated for tracing the alterations in the I-V curve depending on the interaction of enzyme and MoS_2 flake.

2.2.1. Raman spectroscopy measurements

Here, as mentioned previously, CVD grown MoS_2 flakes on SiO_2/Si substrates are used for enzyme experiments. By taking Raman spectroscopy (Raman and PL spectra) and AFM measurements, the MoS_2 flakes are ensured to be monolayer.

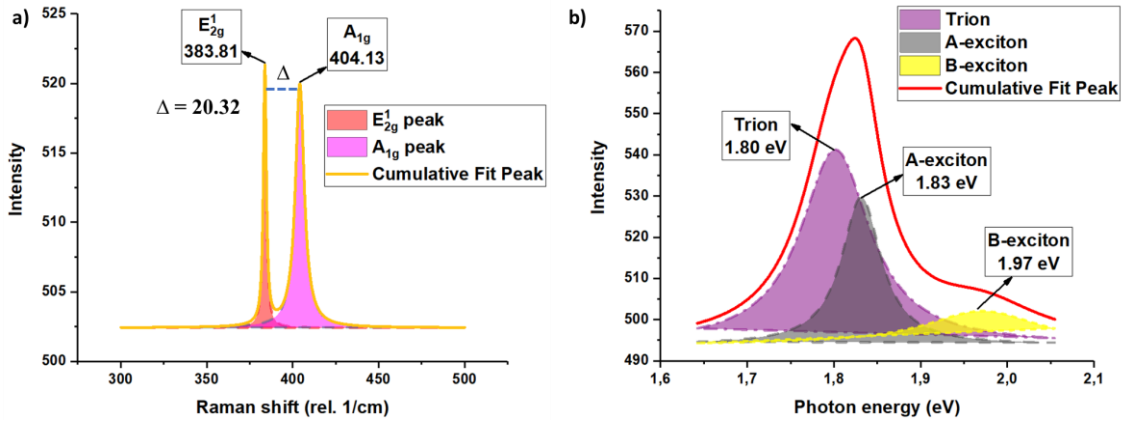

Figure 2.15. *a) Raman and b) PL spectrum of as-grown MoS_2 flake*

After the measurements of the Raman and PL spectra of the as-grown MoS_2 flakes are completed, the enzyme solution is prepared for the immobilization step. The enzyme solution is prepared by mixing 3 mL DI-water and 1 mg enzyme powder (H_2O_2: horseradish peroxide) by using a sonicator tool. After that, by the help of the adjustable pipette, 10 µL of this solution is dropped on the MoS_2 flakes which are directly grown on SiO_2/Si substrate by the assistance of the glass. And enzyme solution is left to dry out on the MoS_2 flakes for approximately 20 minutes. And followingly, PL and Raman mappings of the MoS_2 flakes are taken from the area where the enzyme solution is dropped on. Here, the measurement parameters are kept the same as the as grown parameters where the integration time is 0.5 second and accumulation is 10 and the laser power is 50 µW.

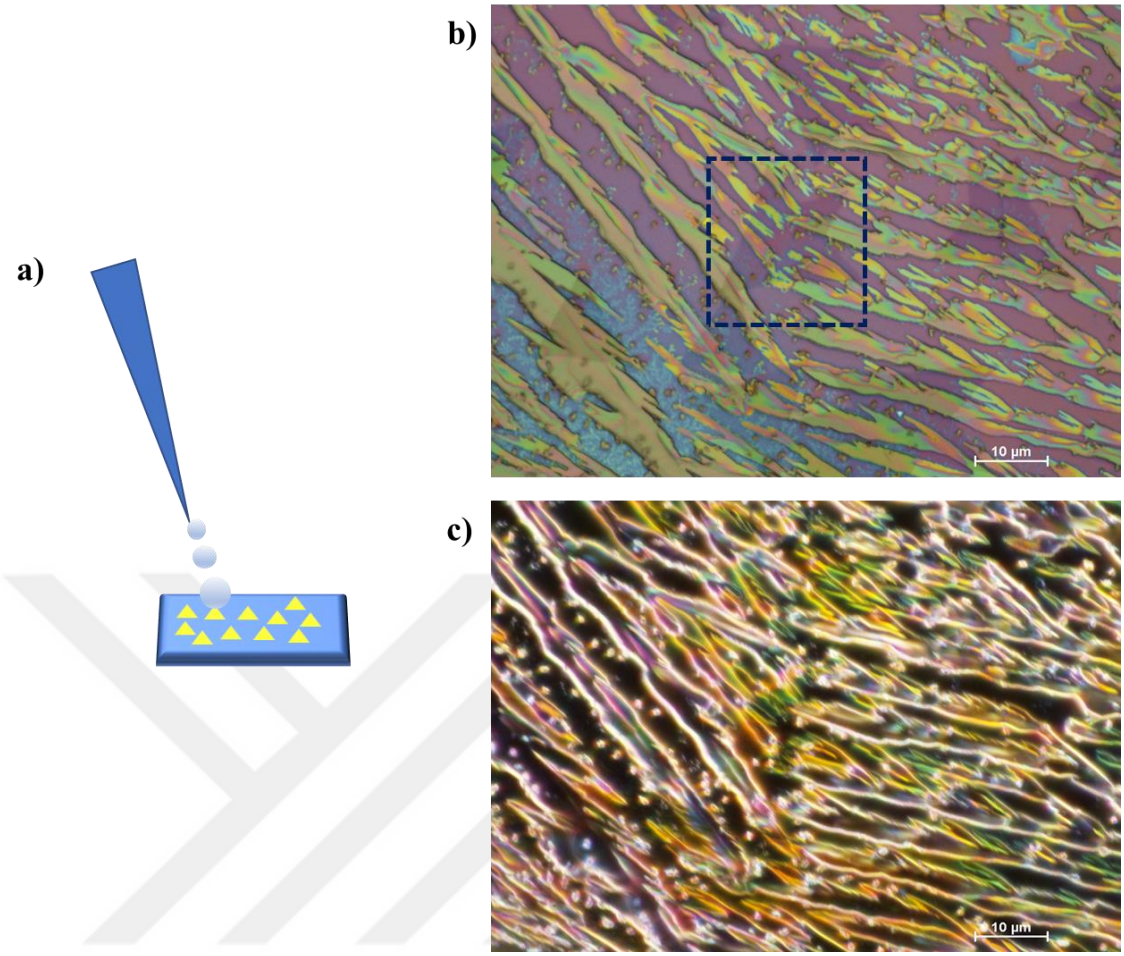

Figure 2.16. *a) 10 µL of Enzyme solution is dropped on the MoS_2 flakes which are grown on SiO_2/Si substrate. b) The bright field image and c) the dark field image of the area where the enzyme solution is dropped*

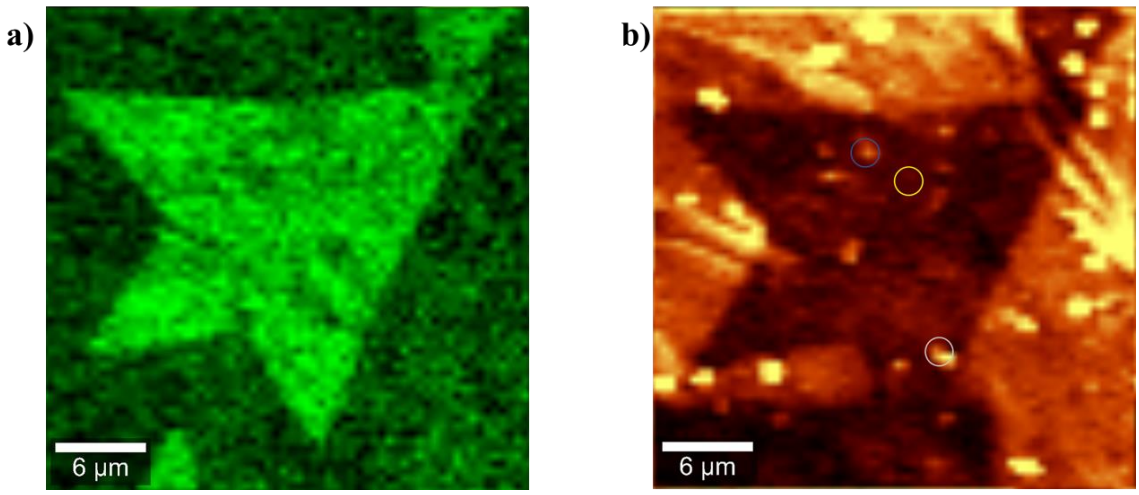

Figure 2.17. *a) Raman and b) PL mapping of the MoS_2 flake which is cover by the dried enzyme solution.*

After finishing with the Raman and PL mapping of the immobilized MoS_2 flakes, the dried enzyme is washed away by using DI water. The washing procedure takes place in three steps. First step: 20 mL DI water is dropped on the immobilized area and waited 5 minutes. Secondly, the substrate is hold with the angle of 45^o and 20 mL DI-water is dropped two times more. As a final step, 50 mL DI-water is dropped on the same area and it is let the whole droplet to fall on a clean SiO_2/Si substrate. This procedure is illustrated in the figure below as representing first step, a; second step, b; and final step, c.

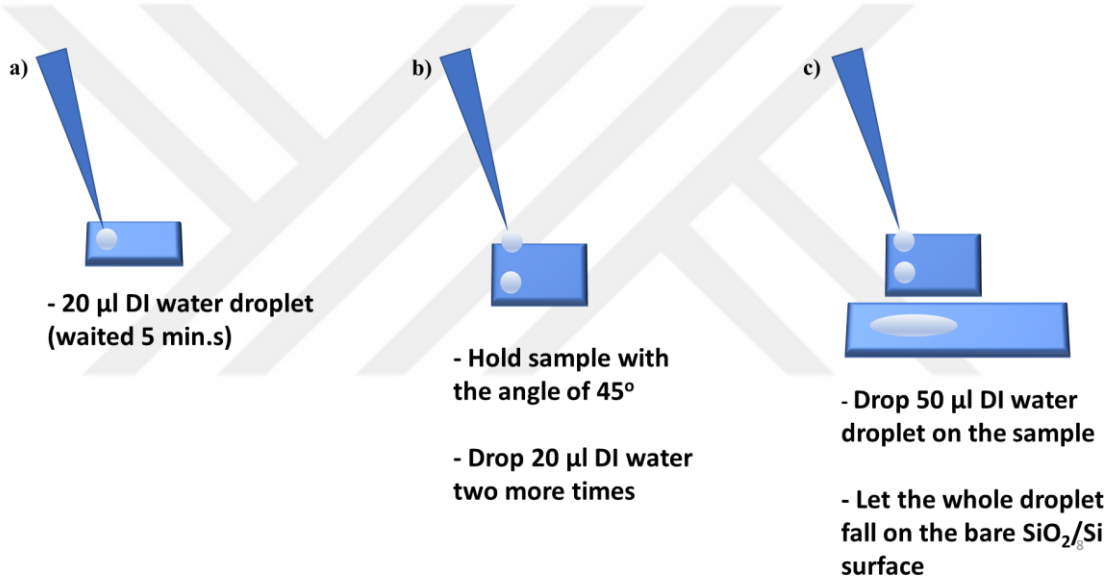

Figure 2.18. *The washing procedure of the immobilized area*

After finishing with the cleaning procedure, the samples are left to dry out again. Later on, the Raman and PL mapping measurements are repeated with the same parameters for the same MoS_2 flakes as both as-grown and immobilized ones. After completing the measurements, the sample with MoS_2 flakes has been washed with DI water one more time with the same washing procedure mentioned above. This second-time washing is to make sure that there is no remaining unbounded enzyme on the surface of MoS_2 flakes. Also, it is thought that it might be helpful for understanding the change

on Raman and PL spectra of the monolayer MoS_2 flakes as the number of washing is increased.

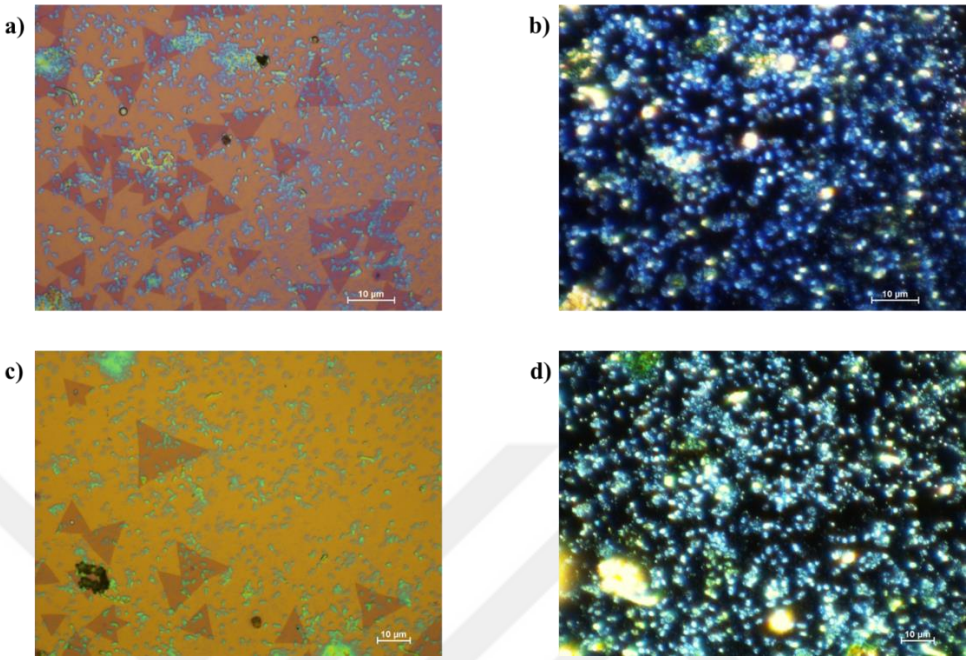

Figure 2.19. *a) The bright field and b) the dark field image of the MoS_2 flakes after washing procedure is applied. c) The bright field and d) the dark field of the MoS_2 flakes after the washing procedure is applied for the second time*

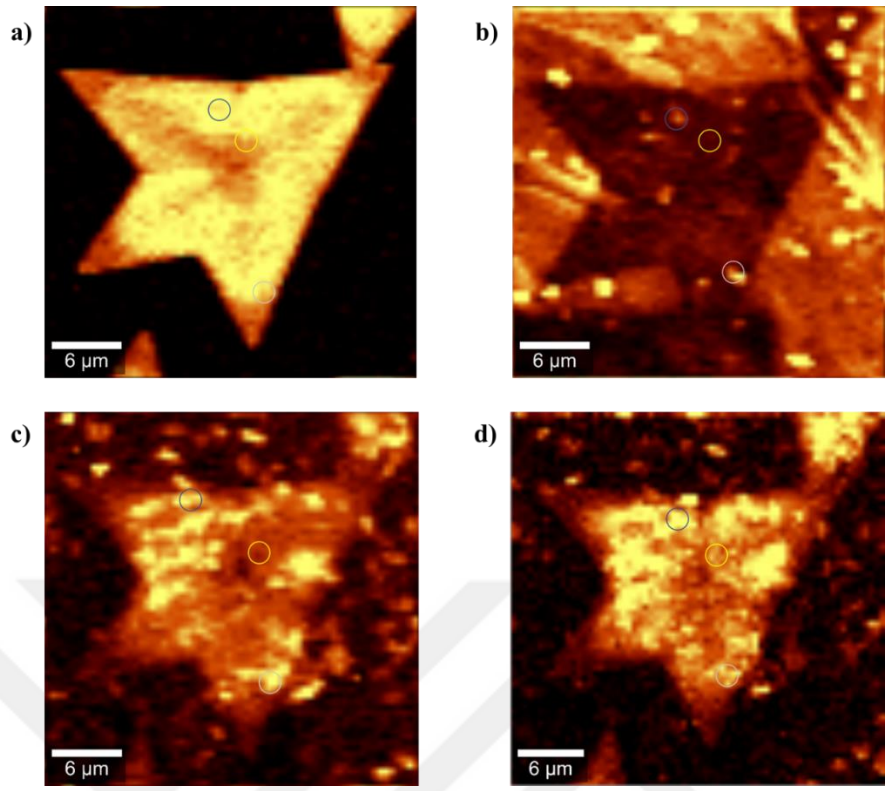

Figure 2.20. *The PL mapping of the a) as-grown MoS_2 flake, b) immobilized MoS_2 flake, c) washed MoS_2 flake, and d) washed MoS_2 flake for the second time*

Above, the images of the PL mapping of the MoS_2 flakes which are in the interaction with the enzyme solution are shown. The bright areas in the Figure 2.19 c and d represents the remaining parts from the enzyme solution after washing procedure is applied. It is seen that in some parts as the more washing is applied the more brightness increases. This occasion may also affect in opposite way because when washing procedure is applied to the enzyme solution, it may sweep away the cohered enzymes from the surface of the MoS_2 flakes. In the PL measurements, it is seen that the PL intensity of the MoS_2 flakes changes with both immobilization and after washing procedures. However, since the washing procedure is not fully controllable, the PL intensity changes cannot be ensured.

Instead of PL intensity changes, it is focused on the alterations in the characteristic peaks of MoS_2 material. The effects of the immobilization and washing procedures on PL peaks are investigated. It is observed that the changes mostly occur on the Trion peak. It is commented that this is because of the hole-electron mismatch existed in the Trion peak, one hole-two electrons or one electron-two holes. The A- and B- exciton peaks are barely

affected depending on the hole-electron pair. In the figure below, the changes in the PL peaks are compared through the as-grown, immobilized and washed MoS_2 flakes.

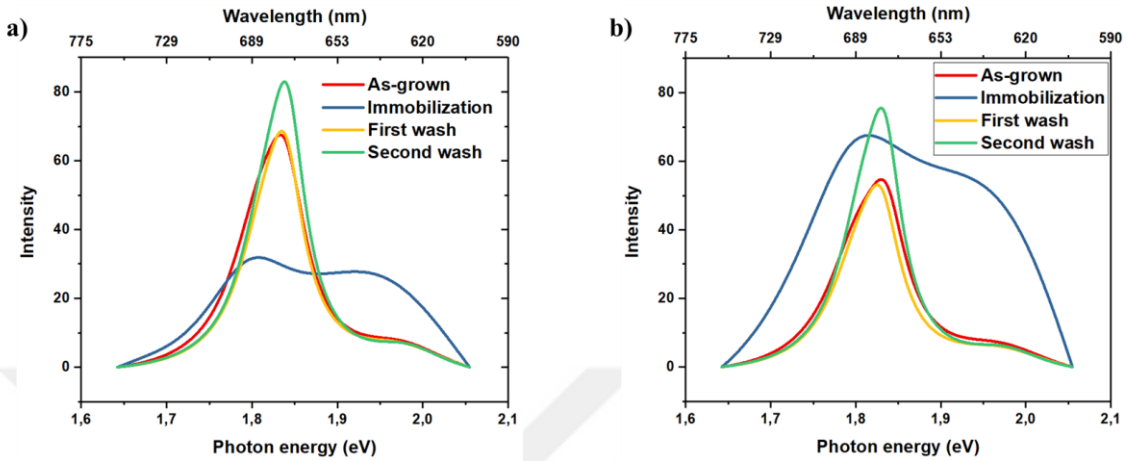

Figure 2.21. *The PL measurements of the MoS_2 flake in interacting with enzyme solution. The measurements are taken from the same flake but different locations*

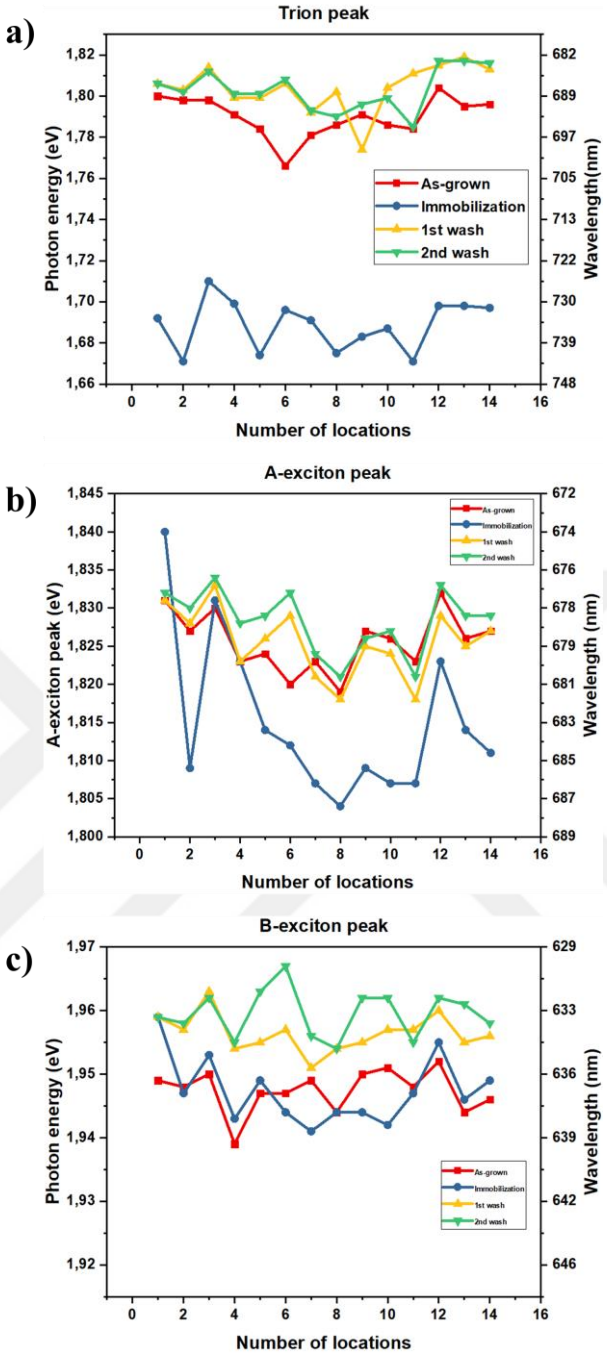

Figure 2.22. *The changes occur in a) Trion, b) A-exciton, b) B-exciton PL peaks.*

Moreover, full width half maximum (FWHM) changes of the PL peaks are separately examined. It is observed that when the MoS_2 flakes are immobilized by the enzyme solution, the FWHM of the PL peaks is increasing. However, when the washing procedure is applied on the MoS_2 flakes, the FWHM is starting to decrease. The more the flakes are washed the more the FWHM of the PL peaks decreases.

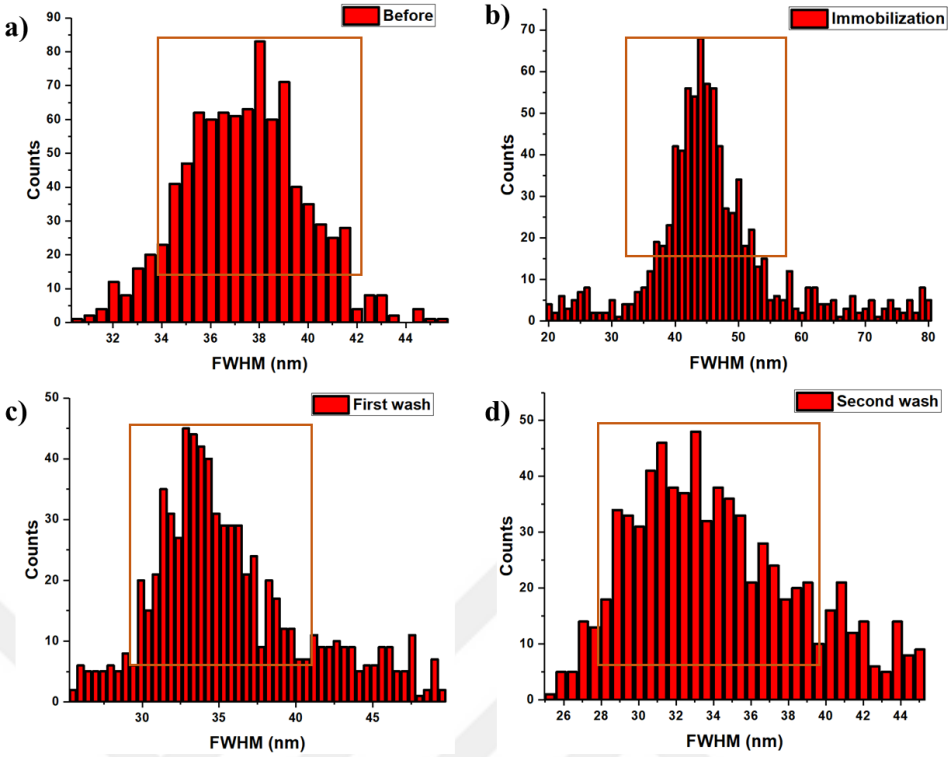

Figure 2.23. *FWHM changes in Trion PL peak of the monolayer MoS_2 flake*

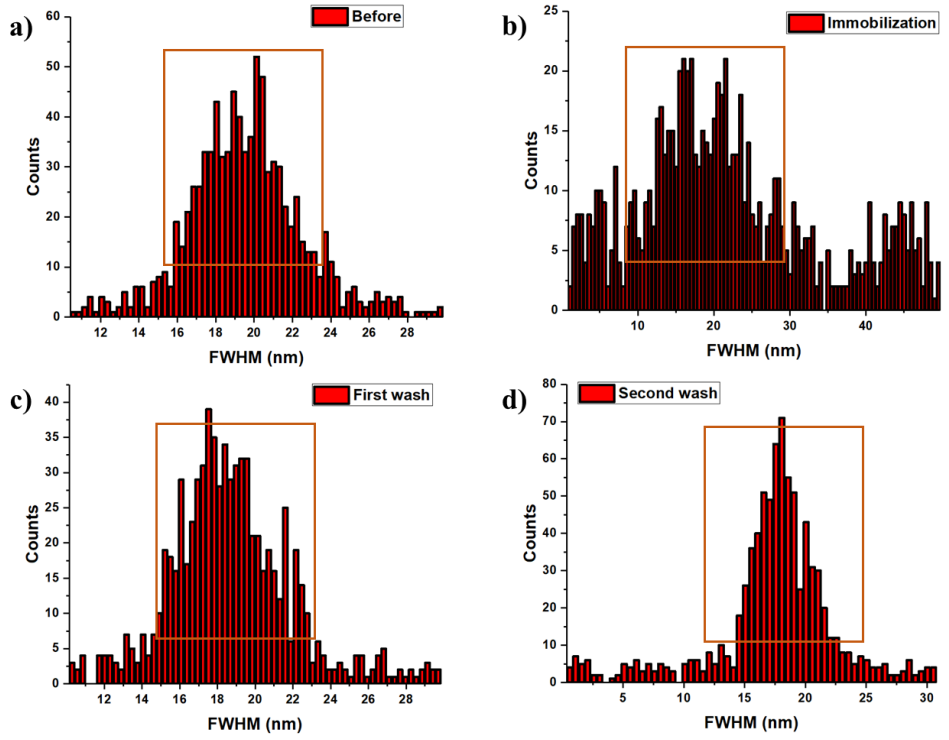

Figure 2.24. *FWHM changes in A-exciton PL peak of the monolayer MoS_2 flake*

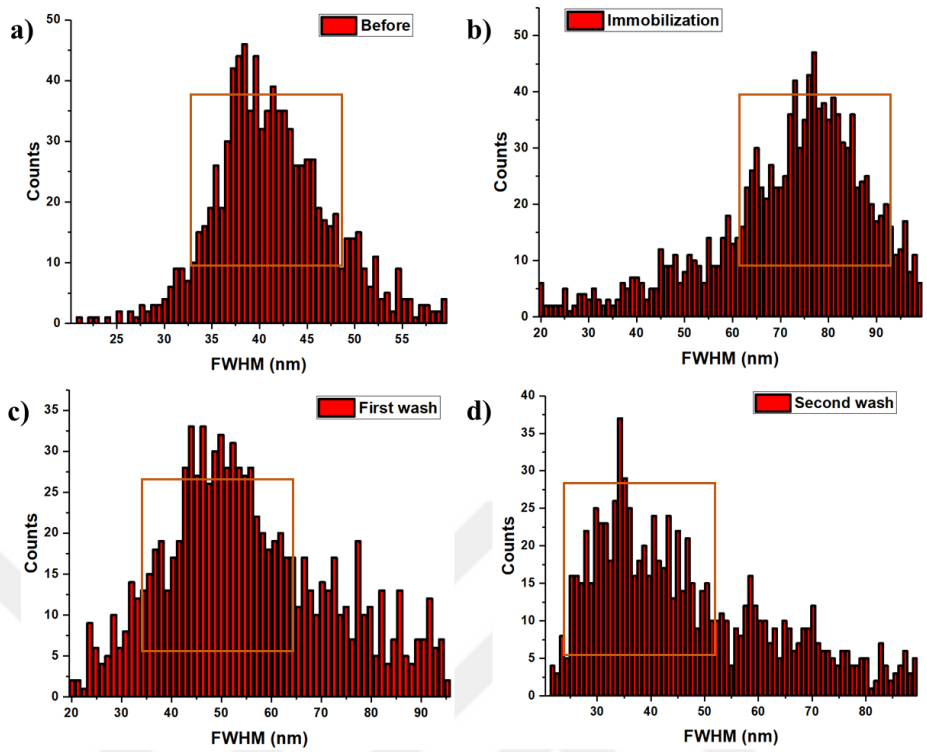

Figure 2.25. *FWHM changes in B-exciton PL peak of monolayer MoS_2 flake*

As the FWHM changes in the PL peaks of monolayer MoS_2 flake are shown in the figures above, it is recognized that the interaction of the MoS_2 flakes with the enzyme solution causes shifts. Especially in Trion and B-exciton peaks, the FWHM of the peaks are increasing after immobilization. After washing procedure is applied to the flake, the FWHM of the peaks is starting to decrease and becomes narrower at some points. The changes in FWHM value of the A-exciton PL peak are slightly observed. These changes in FWHM values of the Trion and B-exciton PL peaks obviously show that the enzyme solution and MoS_2 flakes have an effective interaction.

Followingly, the Raman spectra changes based on the interaction of the enzyme solution and MoS_2 flakes are examined. First of all, it is seen that there are observed new Raman peaks when the immobilization is applied on the MoS_2 flake. These new peaks are expected to be caused by the enzyme solution. After washing procedure, it is observed that the existing Raman peaks are starting to fade away.

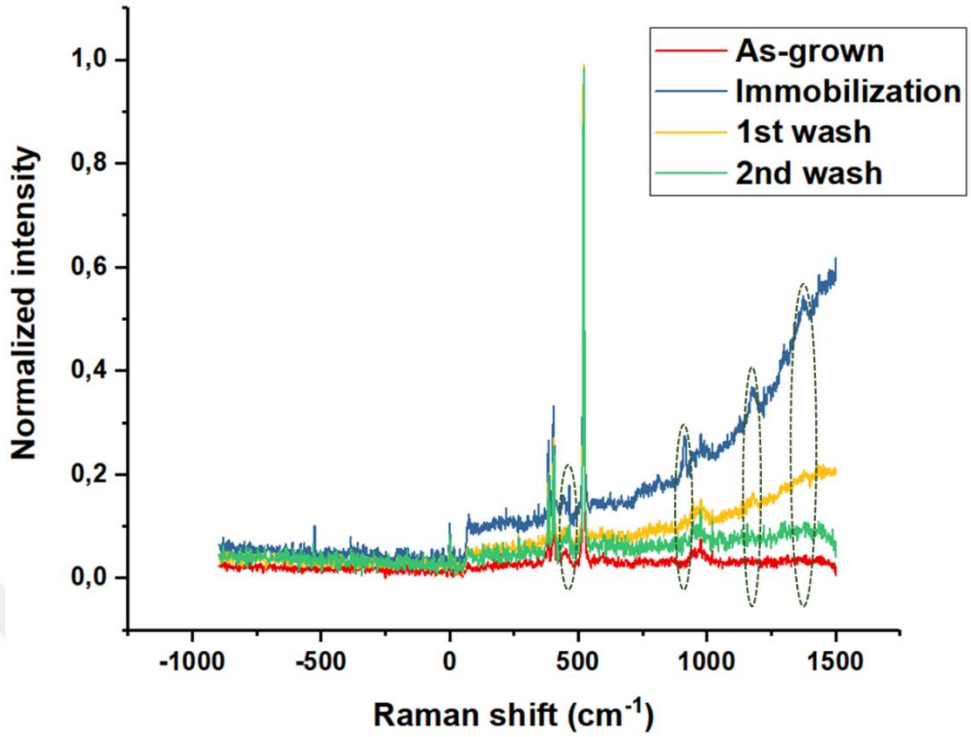

Figure 2.26. *The Raman spectra of the as-grown, immobilized, and washed MoS_2 flake, which is taken from the same point on the same flake*

Then, the characteristic Raman peaks of the MoS_2 material are also taken into consideration. It is seen that the positions of the peaks don't change, which means that the MoS_2 flakes still have the monolayer properties. After the $E_{2g}{}^1$ and A_{1g} peaks are normalized, there occur no shifts at the peak positions of both Raman peaks so the difference between these two peaks remains almost the same.

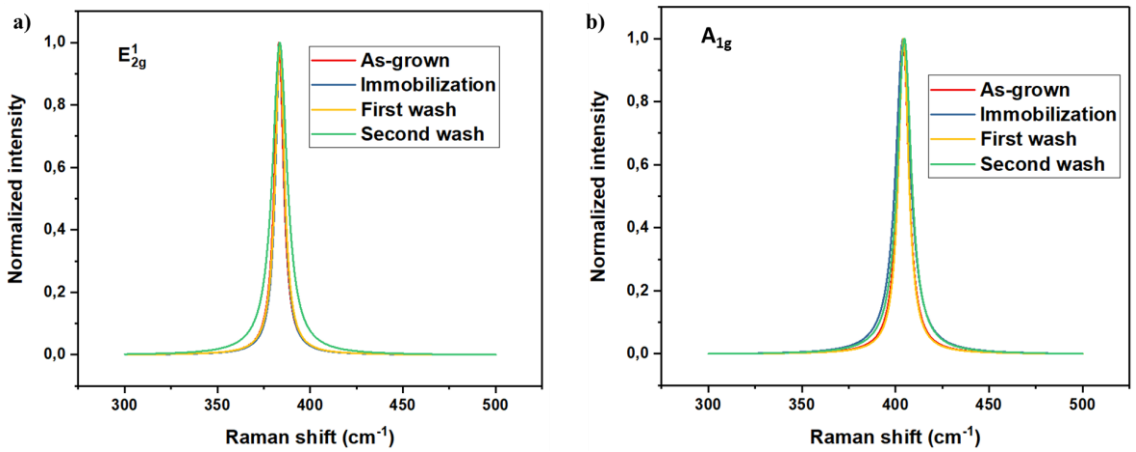

Figure 2.27. *The normalized a) E_{2g}^1 and b) A_{1g} Raman peaks*

2.2.2. The spectrophotometer measurements

The spectrophotometer tool is used for the measurements of the activity of the enzymes. The enzymes are activated by providing an ideal environment. This environment includes the pH value of the solution and certain amount of chemical solutions for enzyme activation. In this part, after monolayer MoS_2 flakes are grown by CVD on glass substrate and ready to harvest, the chemical solutions are prepared for enzyme activation.

2.2.2.3. Preparing the chemical solutions

Firstly, 0.208 mg H_2O_2 is measured and it is mixed with 10 ml 2 M H_2SO_4 solution. Later, 35 ml $KMnO_4$ is added to the mixture. The final mixture is titrated for some period. Afterwards, 0.03 g $Na_2C_2O_4$ is added into 50 ml DI-water and mixture with 2.5 ml 2 M H_2SO_4. This final mixture is titrated by adding 3.6 ml $KMnO_4$ solution. At the end, the grade of purity of the H_2O_2 solution is calculated and the final results are checked if the measured values of the chemicals are matching with the percentage of the H_2O_2 solution which is commercial.

$$\text{Normality} = (0.03\ \text{g}\ Na_2C2O_4) / 134 \times 2 \times 1000 / (3.6\ \text{ml}\ KMnO_4) = 0.124\ N$$

$$\%\ H_2O_2 = (0.124 \times 35\ \text{ml}\ KMnO_4 \times 1.701) / (0.208\ \text{g}\ H_2O_2) = \%\ 35.5$$

As a result, it is seen that the calculation is matching with the commercial H_2O_2 solution (%34-36), which is used in the experiments.

Later on, it is continued with the preparation of the leucocrystal violet (LCV) solution. Approximately 0.02 g LCV is added to 5o ml 0.06 M HCl acid. It is decided by the calculations of:

$$m_{HCl} = 0.06\ M \times 0.05\ L \times (36.5\ g/mol) = 0.1095\ g\ HCl$$

$$= 0.1095\ g\ HCl \times (100 / 37) = 0.296\ g$$

$$m_{LCV} = 0.001\ M \times 0.05\ L \times (373.53\ g/mol) = 0.019\ g\ LCV$$

- Molecular weight of LCV is 373.53 g/mol.

Next, the buffer solution is prepared. KH_2PO_4 and H_3PO_4 solutions are used to prepare the buffer with the pH value of 4.1. The molecular weight (MW) of KH2PO4 is noted as 136.08 g/mol for 200 ml buffer solution.

$$M_{KH_2PO_4} = M \times V \times MW = 1\ M \times 0.2\ L \times 136.08\ g/mol = 27.2\ g$$

27.2 g of KH_2PO_4 is dissolved in 150 ml DI-water and by adding small drops of H_3PO_4 acid inside this mixture, pH value is adjusted to be 4.1. And, DI-water is added to final volume of 200 ml.

After finishing these solution preparations, horse-radish peroxide (HRP) enzyme is prepared. 0.001 g enzyme is added into 1.5 ml DI-water.

For the activation of the enzyme, the solutions are mixed in the certain quantities. Also, by changing the amount of the H_2O_2 and DI water mixtures, the standard curve is obtained. The different amount of the H_2O_2 and DI water mixture with the other solutions are presented in the table below.

Table 2.2. *The quantities of the solution for standard curve*

DI-water (µl)	H_2O_2 (µl)	Buffer (ml)	LCV (µl)	DI-water (ml)	Enzyme (µl)
140	0	400	50	2400	10
120	20				
100	40				
80	60				
60	80				
40	100				
20	120				
0	140				

Each solution is mixed in separate tubes and these different 8 tubes are prepared for absorbance measurements. The measurements are made with the wavelength of 592 nm which corresponds to highest luminescence value between the range of 200 -750 nm. The obtained results are presented in the table below.

Table 2.3. *The absorbance measurements of the enzyme solutions*

Amount of H_2O_2	Absorbance value 1	Absorbance value 2
0	0	0
20	0.139	0.161
40	0.333	0.338
60	0.459	0.516
80	0.644	0.647
100	0.799	0.826
120	1.013	0,989
140		1.125

Table 2.4. *The standard curve calculations for 10 ppm H_2O_2*

Amount of H_2O_2 (µl) $X_{µl}$	Equation	Results (ppm)
0	($X_{µl}$ x 10 ppm) / (140 µl)	0,000
20		1,429
40		2,857
60		4,286
80		5,714
100		7,143
120		8,571
140		10,000

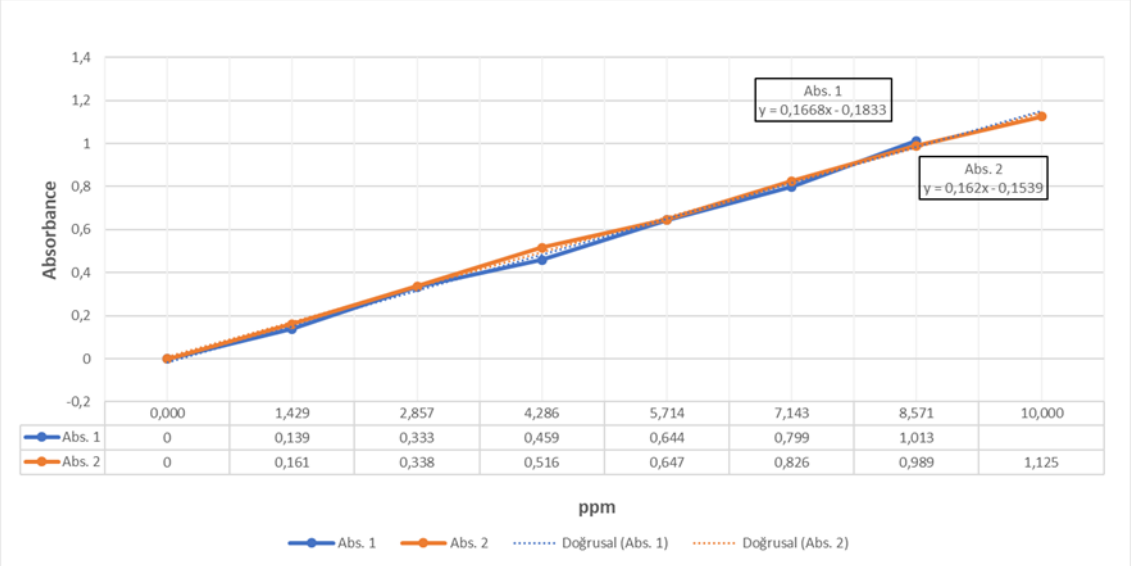

Figure 2.28. *The standard curve of the activated enzyme solution*

In the standard curve graph, it is seen that the slope of both absorbance measurements related to activated enzyme solution including different amount of H_2O_2 and DI water mixtures has the almost same value.

Here, after the standard curve is obtained, the MoS_2 experiments take place. 100 mL H_2O_2 (10 ppm H_2O_2) and 40 mL DI water is mixed. Later, 400 mL buffer and 50 mL LCV are added into the mixture. After that, two tubes are prepared without adding neither enzyme nor MoS_2 flakes. These tubes are prepared as blank tubes which includes only

H_2O_2, DI water, buffer and LCV. Besides blank tubes, 5 more tube are prepared. In these tubes, 10 mL enzyme solution added. As a final step, MoS_2 samples are added into the final solution and mixed. Followingly, spectrophotometer measurements are taken with the laser source of 592 nm wavelength. As a result of these measurements, it is found that, there is no direct impact of MoS_2 samples on the enzyme activity. This might be caused by the low amount of MoS_2 flakes in the solutions. They might be hard to be detected. Or they only interact with the enzymes on the substrate surface instead of the solution. These are some of the results pf the measurements: blank tube: 0, only enzyme: 0.802, MoS_2 sample:0.878, washed-MoS_2 flakes: 0.778, washed MoS_2 flakes-2: 0.803, only MoS_2 sample: 0.051,

2.2.3. FET device fabrication for I-V characterization

In this section, Four-probe method is used for I-V characterization of the interaction of the monolayer MoS_2 flake and enzyme. Here, first of all the grown monolayer MoS_2 flakes on glass substrate are transferred onto SiO_2/Si substrate for I-V characterization of the as-grown MoS_2 flakes.

2.2.3.1. Transfer of the monolayer MoS_2 flakes onto SiO_2/Si substrate

As-grown monolayer MoS_2 flakes on glass substrate are coated with the PMMA polymer by using spin-coater tool. PMMA is dropped on the glass substrate till it covers all the surface properly. Later then, it is spun for 50 seconds by using spin-coater tool. Followingly, it is heated at 130 ^oC on the heater for 2 minutes. After that, the edges of PMMA adhered on the glass are cut with the prong of the curved knife. Then, it is immersed in water to separate the adhered PMMA layer from the glass surface. After completing this separation process, the fishing is applied. At this step, the PMMA layer which is swimming on the water surface is fished carefully to cling onto the surface of the SiO_2/Si substrate. Afterwards, it is annealed at 70 ^oC for some time for the complete adhesion of the PMMA layer onto SiO_2/Si substrate. Finally, after annealing process, the sample is put into the acetone solution at 50 ^oC to get rid of the PMMA layer only. By doing so, the monolayer MoS_2 flakes remains on the surface of the SiO_2/Si substrate while PMMA polymer layer dissolves in the acetone solution.

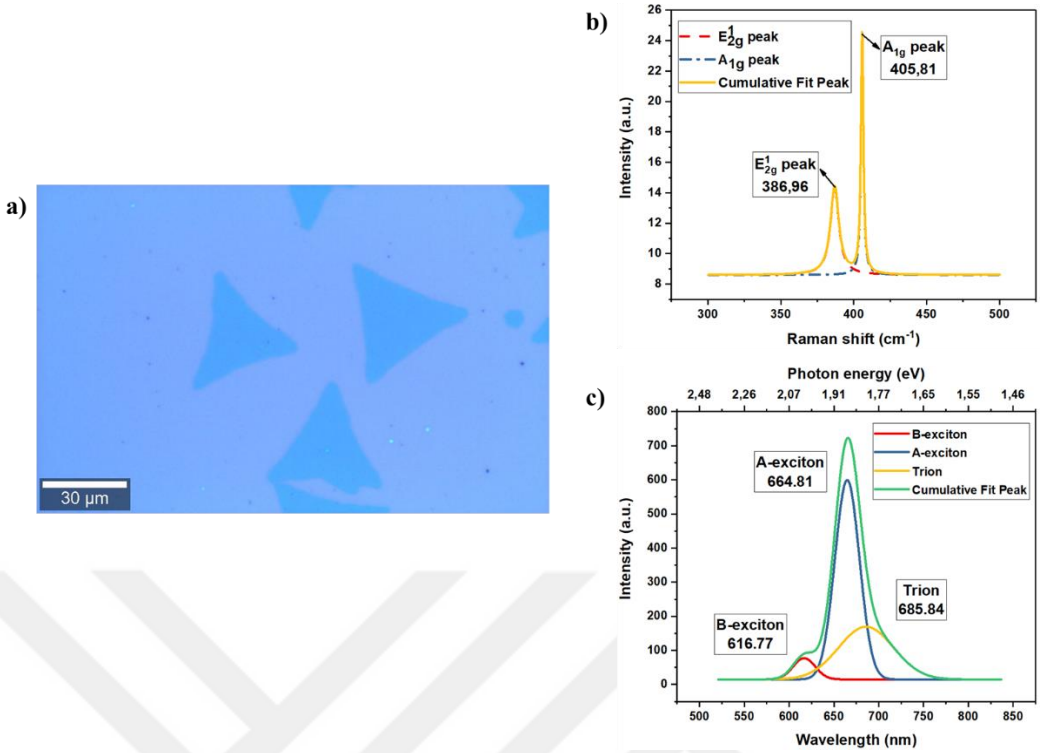

Figure 2.29. *a) The optical image, b) Raman and c) PL spectrum of theMoS_2 flakes transferred onto SiO_2/Si substrate.*

2.2.3.2. Photolithography process

Photolithography process is the second step for the I-V characterization while fabricating a FET device. Here, firstly, the transferred monolayer MoS2 flakes onto SiO2/Si substrate are coated with the AZ5214E photoresist by using the spin coater tool. It is coated at the 6000 rpm which provides the thickness of approximately 1.4 µm. After coating, it is annealed at 110 ºC for 50 seconds and it is exposed under UV light for 10 seconds. After explosion, it is submerged into the developer solution which is prepared by mixing 4 ml AZ351B Developer solution and 16 ml DI-water.

2.2.3.3. Coating process by E-beam tool

As a final step in fabrication a FET device, the developed samples are coated with 10 nm Ti and 100 nm Au as the contact fields. For coating process, E-beam tool is used. In the E-beam process, firstly 20 mA is applied to the holder to coat 10 nm Ti material with the rate of 0.2-0.3 A/sec under 4.2 micro-Torr pressure. Followingly, the current of 20 mA is applied to the Au holder to coat 100 nm Au onto top of the Ti material with the rate of 0.1-0.2 A/sec under 2.6 micro-Torr pressure at the beginning for 2 minutes. Then,

the current is increased to 26 mA for Au coating with the rate of 0.8 A/sec under 3.5 micro-Torr for5 minutes. And as a final step, the current is increased to 28 mA for coating Au with the rate of 1.1-1.2 A/sec under 3.7 micro-Torr till reaching to the final thickness. Thus, the coating process is completed.

2.2.3.4. Lift-off process

After the coating process, lift-off process is applied. For the lift off process, the coated sample is submerged into to acetone solution at 70 ^{o}C. It is waited inside the acetone till the remaining photoresist parts are removed. After being sure that the removal step is totally completed, the sample is taken out of the acetone and washed with iso-propanol and dried with nitrogen.

Afterwards, the samples are annealed in the CVD furnace under nitrogen atmosphere, 500 sccm nitrogen is purged inside the quartz tube, under the 200 Torr pressure at 200 ^{o}C for 120 minutes. This is the final step for the fabrication of the FET device.

2.2.4. I-V measurement

For measuring I-V curve of the fabricated device by using monolayer MoS2 flake, four probe method is used. This four-probe measurement station has been built in our laboratory by hand. One of the probes is used as the gate the others are source and drain. The remaining one is used for the grounding.

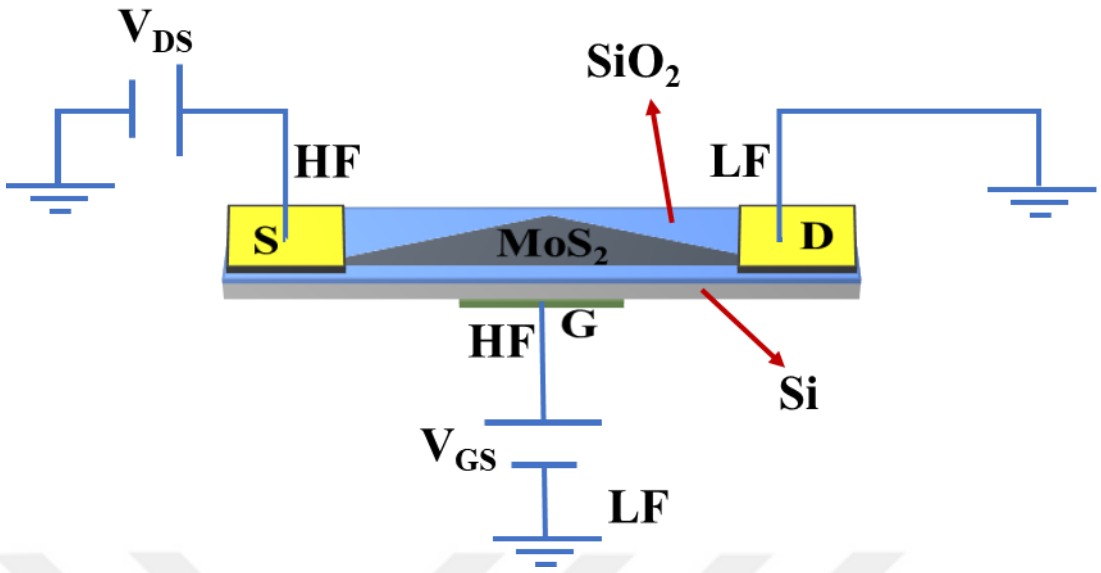

Figure 2.30. *The schematic illustration of the FET device fabricated with a monolayer semiconductor MoS_2 material*

Here, V_{ds} is adjusted to be 5 V and V_{gs} voltage has been swung between -150 V to 150 V. Firstly, the measurements have begun with the as-fabricated devices and are obtained as a function of back gate voltage. The measurements have continued with the immobilizing the same devices. The immobilized devices are washed with DI-water is described in the washing processes part. The measurements are taking place in four sections which are; as-fabricated, immobilized, first wash, and second wash.

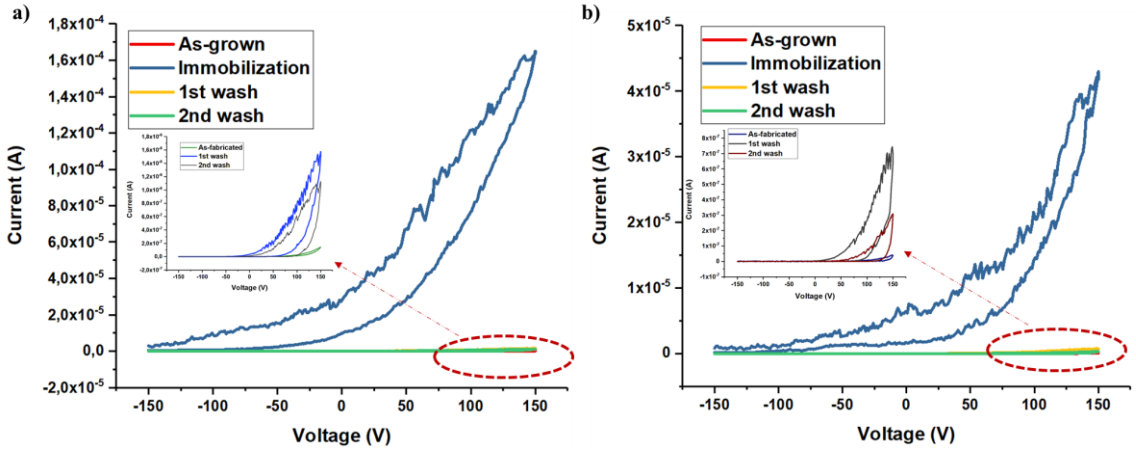

Figure 2.31. *The I_{DS}-V_{GS} curves of the FET device a) under white light and b) under the dark, where V_{DS} is kept as 5 V.*

As it is seen in the graphs of the I-V curves, the performance of the FET device after immobilization process considerably increases. After washing procedures are applied to the device, it is observed that the magnitude of the peak value of the I-V decreases. Notwithstanding, the FET device shows a better performance in comparison to the as-fabricated situation. This results conform with the PL results. Since the PL spectrum of MoS_2 material gives a better result after washing procedure, it is expected the performance of the fabricated FET device to increase.

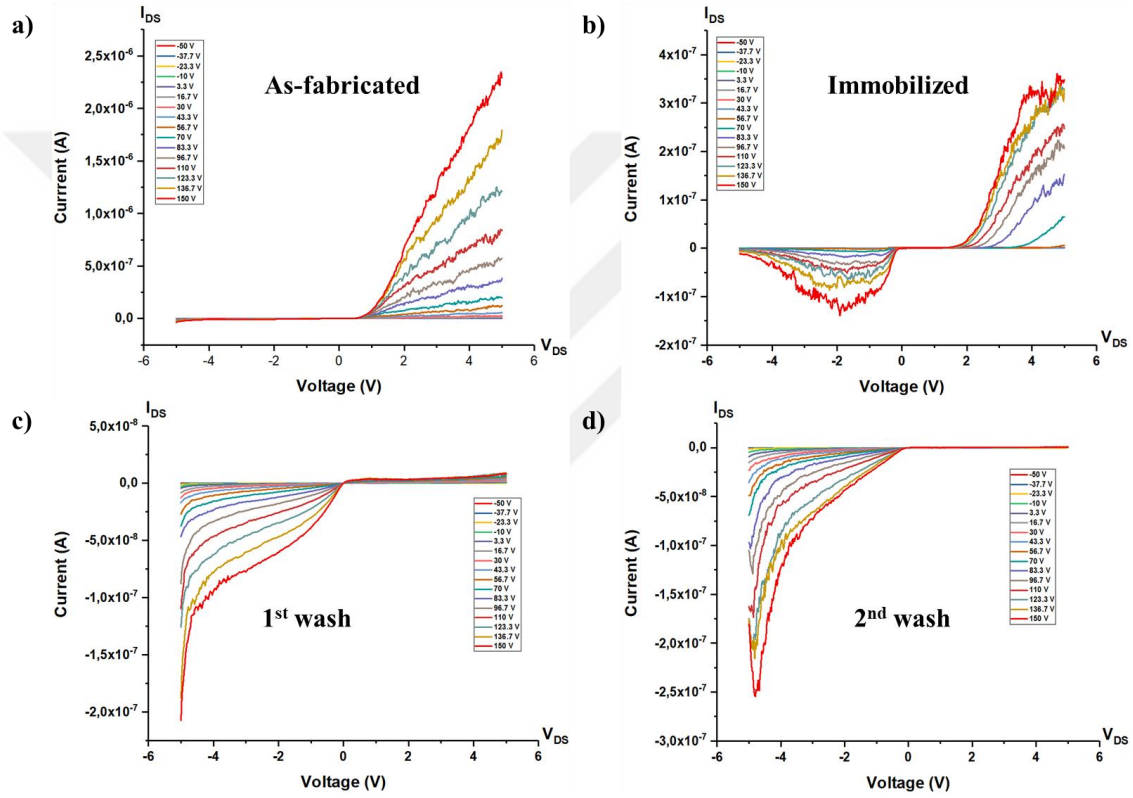

Figure 2.32. *Drain-source current I_{DS} as a function of drain-source voltage V_{DS} for different values of V_{GS}. The measurements are performed for different situations, as fabricated, immobilized, 1st and 2nd washes, under the same circumstances where the white light source is used at the room temperature*

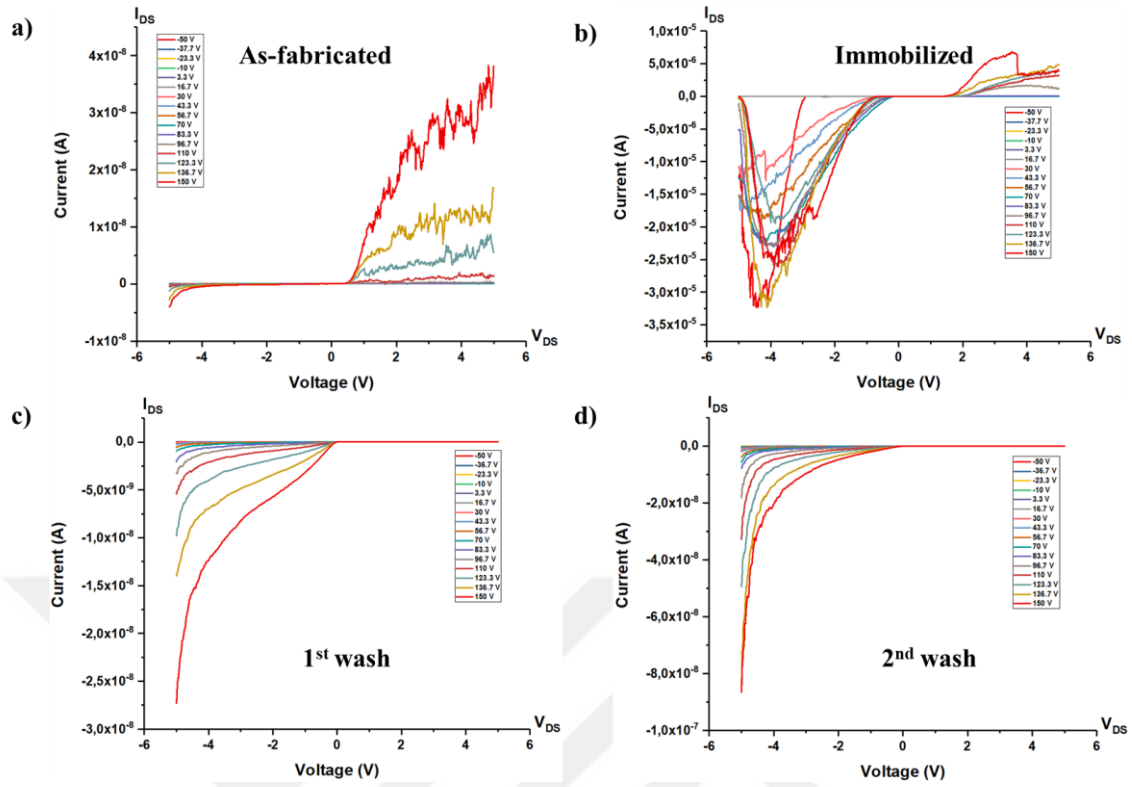

Figure 2.33. *Drain-source current I_{DS} as a function of drain-source voltage V_{DS} for different values of V_{GS}. The measurements are performed for different situations, as fabricated, immobilized, 1st and 2nd washes, under the same circumstances where no light source is used at the room temperature*

After one month, the measurement of the FET device, which is washed two times, is performed. It is observed that the performance of the device gets better in comparison to the performance after 2nd wash. This measurement can indicate that the MoS_2-based FET devices can be reused. Along with, the performance of the device may also reach to the as-fabricated performance or it can remain lower than as-fabricated performance but better than 2nd wash performance.

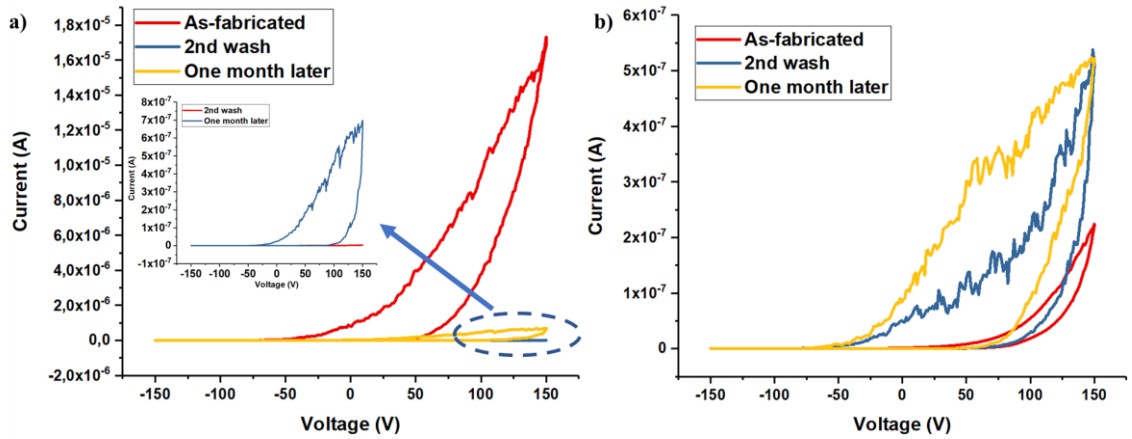

Figure 2.34. *The comparison of the performance of the MoS_2-based FET device depending on the time under white light source*

Even though there are some unexplained variations in the characteristic I_{DS}-V_{DS} curves, it can be said that the enzyme immobilization may work for the detection of the HRP enzyme. It is also observed that the washing procedure is critical for FET measurements because it might also cause damages on the MoS_2 flakes such as cracks, tears, etc. These damages can affect the performance of the fabricated FET device in negative way. For example, decreasing in the FET device performance or unexplained jumps in the I-V curve results might be encountered. To be able to prevent these occasions, the washing procedure must be occurred in a more stabilized way which means eliminating the vibrations during washing process.

The reason for using or not using light source is to distinguish the behavior of the enzyme-monolayer MoS_2 structure under distinct circumstances. It is observed that there is also increase in the I-V value of the immobilized FET device when no light source is used.

3. CONCLUSION

In this thesis, monolayer TMDC materials (MoS_2, $MoSe_2$, WS_2) are successfully grown by CVD system. Among these TMDCs, it is focused on monolayer MoS_2 material to be used for the biosensor application. First, monolayer MoS_2 flakes are directly grown on SiO_2/Si substrates by the assistance of a piece of glass to be able to have a large surface. These grown flakes are used for the observation of the photonics properties of the monolayer MoS_2 flakes with the interaction of the enzyme (HRP) solution. It is concluded that the interaction of the enzyme solution with the monolayer MoS_2 flakes has effect on the PL and Raman measurements. The immobilization process causes shifts on the PL peaks and also the FWHM values of the PL peaks. Also, new Raman peaks are appeared after the interaction between MoS_2 flakes and enzyme solution. Later, monolayer MoS_2 flakes are grown on a piece of glass (2 cm x 2 cm) and transferred on SiO_2/Si substrate for the FET fabrication. When I-V graphs are considered, it is observed that the interaction of the enzyme solution and MoS_2 flake causes increasement in the I-V measurement in comparison to the as-fabricated situation. After washing procedures are applied, there is a decrease observed on the I-V measurement. This explains that the immobilization of the MoS_2 flakes by HRP enzyme solution can be distinguishable by the help of the I-V measurements. Moreover, after one month, when the measurement is repeated for the "after 2^{nd} wash" situation, it is seen that the device performance reaches to its initial conditions which is almost the same as the as-fabricated situation. Hence, it can be said that the MoS_2-based FET device can be reused. Here, it can be said that monolayer MoS_2 material can be a promising candidate for the sensing application of the HRP enzyme in both photonic and electronic ways.

4. FUTURE PROSPECTS

Using monolayer MoS_2 structures for the detection of the enzymes seems to be promising. The detection can be in the photonic, PL and Raman measurements, or electronic, device fabrication, prospects. Here, the MoS_2 structure is used as an initial material to pave the way for the other monolayer TMDC or two-dimensional materials which may have a better potential for the detection of the enzymes. Also, different kind of properties of monolayer MoS_2 material is benefited as it is mentioned. Therefore, it provides many options for the enzyme applications to be examined. It is not only for enzyme but also for other related areas including proteins, bacteria, or complex organisms. It can be claimed that the application fields of the MoS_2 material depending on its distinctive characteristics can be broaden.

Along with, the family of TMDC materials is very wide. An appropriate candidate from this family can be chosen for the main purpose of the application. Different methods or techniques can be used for different types of detections and purposes.

REFERENCES

[1] Izyumskaya, N., O. Demchenko, D., Avrutin, V., Özgür, Ü., Morkoç, H. (**2014**). Two-dimensional MoS_2 as a new material for electronic devices. *Turk J Phys*, 38

[2] Mas-Ballesté, R., Gómez-Navarro, C., Gómez-Herrero, J., Zamora, F. (2011). 2D materials: to graphene and beyond. *Nanoscale*, *3*(1), 20-30.

[3] Novoselov, K. S., Fal′ko, V. I., Colombo, L., Gellert, P. R., Schwab, M. G., Kim, K. (2012). A roadmap for graphene. *Nature*, *490*, 192.

[4] Arco, L. G. D., Zhang, Y., Kumar, A., Zhou, C. (2009). Synthesis, Transfer, and Devices of Single- and Few-Layer Graphene by Chemical Vapor Deposition. *IEEE Transactions on Nanotechnology*, *8*(2), 135-138.

[5] Castro Neto, A. H., Guinea, F., Peres, N. M. R., Novoselov, K. S., Geim, A. K. (2009). The electronic properties of graphene. *Reviews of Modern Physics*, *81*(1), 109-162.

[6] Zhen, Z., Zhu, H. (**2018**). 1 - Structure and Properties of Graphene. In H. Zhu, Z. Xu, D. Xie, & Y. Fang (Eds.), *Graphene* (pp. 1-12): Academic Press.

[7] Lv, R., Terrones, H., Elías, A. L., Perea-López, N., Gutiérrez, H. R., Cruz-Silva, E., Rajukumar, L. P., Dresselhaus, M. S., Terrones, M. (2015). Two-dimensional transition metal dichalcogenides: Clusters, ribbons, sheets and more. *Nano Today*, *10*(5), 559-592.

[8] Gupta, A., Sakthivel, T., Seal, S. (2015). Recent development in 2D materials beyond graphene. *Progress in Materials Science*, *73*, 44-126.

[9] Choi, W., Choudhary, N., Han, G. H., Park, J., Akinwande, D., Lee, Y. H. (2017). Recent development of two-dimensional transition metal dichalcogenides and their applications. *Materials Today*, *20*(3), 116-130.

[10] Wang, H., Li, C., Fang, P., Zhang, Z., Zhang, J. Z. (2018). Synthesis, properties, and optoelectronic applications of two-dimensional MoS2 and MoS2-based heterostructures. *Chemical Society Reviews*, *47*(16), 6101-6127.

[11] Li, X., Zhu, H. (2015). Two-dimensional MoS2: Properties, preparation, and applications. *Journal of Materiomics*, *1*(1), 33-44.

[12] Splendiani, A., Sun, L., Zhang, Y., Li, T., Kim, J., Chim, C.-Y., Galli, G., Wang, F. (2010). Emerging Photoluminescence in Monolayer MoS2. *Nano letters, 10*(4), 1271-1275.

[13] Radisavljevic, B., Radenovic, A., Brivio, J., Giacometti, V., Kis, A. (2011). *Single-layer MoS2 transistors* (Vol. 6).

[14] Huo, N., Yang, Y., Li, J. (2017). Optoelectronics based on 2D TMDs and heterostructures. *Journal of Semiconductors, 38*(3), 031002.

[15] Lopez-Sanchez, O., Lembke, D., Kayci, M., Radenovic, A., Kis, A. (2013). Ultrasensitive photodetectors based on monolayer MoS2. *Nature nanotechnology, 8*, 497.

[16] Yuk Choi, S., Tung Yip, C., Li, G., Lei, D., Fung, K. H., Yu, S., Hao, J. (2015). *Photoluminescence enhancement in few-layer WS2 films via Au nanoparticles* (Vol. 5).

[17] Wang, X., Gong, Y., Shi, G., Chow, W. L., Keyshar, K., Ye, G., Vajtai, R., Lou, J., Liu, Z., Ringe, E., Tay, B. K., Ajayan, P. M. (2014). Chemical Vapor Deposition Growth of Crystalline Monolayer MoSe2. *ACS Nano, 8*(5), 5125-5131.

[18] Chang, Y.-H., Zhang, W., Zhu, Y., Han, Y., Pu, J., Chang, J.-K., Hsu, W.-T., Huang, J.-K., Hsu, C.-L., Chiu, M.-H., Takenobu, T., Li, H., Wu, C.-I., Chang, W.-H., Wee, A. T. S., Li, L.-J. (2014). Monolayer MoSe2 Grown by Chemical Vapor Deposition for Fast Photodetection. *ACS Nano, 8*(8), 8582-8590.

[19] Liu, B., Fathi, M., Chen, L., Abbas, A., Ma, Y., Zhou, C. (2015). Chemical Vapor Deposition Growth of Monolayer WSe2 with Tunable Device Characteristics and Growth Mechanism Study. *ACS Nano, 9*(6), 6119-6127.

[20] Zhou, H., Wang, C., Shaw, J. C., Cheng, R., Chen, Y., Huang, X., Liu, Y., Weiss, N. O., Lin, Z., Huang, Y., Duan, X. (2015). Large Area Growth and Electrical Properties of p-Type WSe2 Atomic Layers. *Nano letters, 15*(1), 709-713.

[21] Xu, K., Wang, Z., Du, X., Safdar, M., Jiang, C., He, J. (2013). Atomic-layer triangular WSe2sheets: synthesis and layer-dependent photoluminescence property. *Nanotechnology, 24*(46), 465705.

[22] Huang, J.-K., Pu, J., Hsu, C.-L., Chiu, M.-H., Juang, Z.-Y., Chang, Y.-H., Chang, W.-H., Iwasa, Y., Takenobu, T., Li, L.-J. (2014). Large-Area Synthesis of Highly Crystalline WSe2 Monolayers and Device Applications. *ACS Nano, 8*(1), 923-930.

[23] Shi, Y., Li, H., Li, L.-J. (2015). Recent advances in controlled synthesis of two-dimensional transition metal dichalcogenides via vapour deposition techniques. *Chemical Society Reviews, 44*(9), 2744-2756.

[24] Wang, J., Li, G., Li, L. (**2016**). Synthesis Strategies about 2D Materials. In *Two-dimensional Materials - Synthesis, Characterization and Potential Applications*.

[25] Eda, G., Yamaguchi, H., Voiry, D., Fujita, T., Chen, M., Chhowalla, M. (2011). Photoluminescence from Chemically Exfoliated MoS2. *Nano letters, 11*(12), 5111-5116.

[26] Golberg, D. (2011). Exfoliating the inorganics. *Nature nanotechnology, 6*, 200.

[27] Tan, C., Zhang, H. (2015). Wet-chemical synthesis and applications of non-layer structured two-dimensional nanomaterials. *Nature Communications, 6*, 7873.

[28] Brent, J. R., Savjani, N., O'Brien, P. (2017). Synthetic approaches to two-dimensional transition metal dichalcogenide nanosheets. *Progress in Materials Science, 89*, 411-478.

[29] Zhan, Y., Liu, Z., Najmaei, S., Ajayan, P. M., Lou, J. (2012). Large-area vapor-phase growth and characterization of MoS(2) atomic layers on a SiO(2) substrate. *Small, 8*(7), 966-971.

[30] Liu, K.-K., Zhang, W., Lee, Y.-H., Lin, Y.-C., Chang, M.-T., Su, C.-Y., Chang, C.-S., Li, H., Shi, Y., Zhang, H., Lai, C.-S., Li, L.-J. (2012). Growth of Large-Area and Highly Crystalline MoS2 Thin Layers on Insulating Substrates. *Nano letters, 12*(3), 1538-1544.

[31] Elías, A. L., Perea-López, N., Castro-Beltrán, A., Berkdemir, A., Lv, R., Feng, S., Long, A. D., Hayashi, T., Kim, Y. A., Endo, M., Gutiérrez, H. R., Pradhan, N. R., Balicas, L., Mallouk, T. E., López-Urías, F., Terrones, H., Terrones, M. (2013).

Controlled Synthesis and Transfer of Large-Area WS2 Sheets: From Single Layer to Few Layers. *ACS Nano, 7*(6), 5235-5242.

[32] Wu, S., Huang, C., Aivazian, G., Ross, J. S., Cobden, D. H., Xu, X. (2013). Vapor–Solid Growth of High Optical Quality MoS2 Monolayers with Near-Unity Valley Polarization. *ACS Nano, 7*(3), 2768-2772.

[33] Demirtas, M., Odaci, C., Perkgoz, N. K., Sevik, C., Ay, F. (2018). Low Loss Atomic Layer Deposited Al2O3 Waveguides for Applications in On-Chip Optical Amplifiers. *IEEE Journal of Selected Topics in Quantum Electronics, 24*(4), 1-8.

[34] Leskela, M., Ritala, M. (2003). Atomic layer deposition chemistry: recent developments and future challenges. *Angew Chem Int Ed Engl, 42*(45), 5548-5554.

[35] Leskela, M., Ritala, M. (**2002**). Atomic layer deposition (ALD): from precursors to thin film strcutures. *Thin Solid Films, 409*, 138-146.

[36] Johnson, R. W., Hultqvist, A., Bent, S. F. (2014). A brief review of atomic layer deposition: from fundamentals to applications. *Materials Today, 17*(5), 236-246.

[37] Varghese, N., Ghosh, A., Voggu, R., Ghosh, S., Rao, C. N. R. (2009). Selectivity in the Interaction of Electron Donor and Acceptor Molecules with Graphene and Single-Walled Carbon Nanotubes. *The Journal of Physical Chemistry C, 113*(39), 16855-16859.

[38] Pollard, A. J., Kumar, N., Rae, A., Mignuzzi, S., Su, W., Roy, D. (2014). Nanoscale optical spectroscopy: an emerging tool for the characterization of graphene and related 2-D materials. *J. Mat. NanoSci, 1*, 39-49.

[39] Butler, H. J., Ashton, L., Bird, B., Cinque, G., Curtis, K., Dorney, J., Esmonde-White, K., Fullwood, N. J., Gardner, B., Martin-Hirsch, P. L., Walsh, M. J., McAinsh, M. R., Stone, N., Martin, F. L. (2016). Using Raman spectroscopy to characterize biological materials. *Nat Protoc, 11*(4), 664-687.

[40] Liang, F., Xu, H., Wu, X., Wang, C., Luo, C., Zhang, J. (2018). Raman spectroscopy characterization of two-dimensional materials. *Chinese Physics B, 27*(3).

[41] Dong, Z., Xu, H., Liang, F., Luo, C., Wang, C., Cao, Z. Y., Chen, X. J., Zhang, J., Wu, X. (2018). Raman Characterization on Two-Dimensional Materials-Based Thermoelectricity. *Molecules, 24*(1).

[42] O'Brien, M., McEvoy, N., Hanlon, D., Lee, K., Gatensby, R., Coleman, J. N., Duesberg, G. S. (2015). Low wavenumber Raman spectroscopy of highly crystalline MoSe2grown by chemical vapor deposition. *physica status solidi (b), 252*(11), 2385-2389.

[43] Lee, J.-U., Kim, M., Cheong, H. (2015). Raman Spectroscopic Studies on Two-Dimensional Materials. *Applied Microscopy, 45*(3), 126-130.

[44] Abi Munajad, C. S., Suwarno. (2018). Fourier Transform Infrared (FTIR) Spectroscopy Analysis of Transformer Paper in Mineral Oil-Paper Composite Insulation under Accelerated Thermal Aging. *Energies, 11*(2).

[45] ThermoNicoletCorporation. (2001). Introduction to Fourier Transform Infrared Spectrometry. 1-8.

[46] Dole, M. N., Patel, P. A., Sawant, S. D., Shedpure, P. S. (2011). Advance applications of Fourier transform infrared spectroscopy. *Int. J. Pharm. Sci. Rev. Res, 7*(2), 159-166.

[47] Jagtap, R., Ambre, A. (**2006**). *Atomic force microscopy (AFM): Basics and its important applications for polymer characterization: An overview* (Vol. 13).

[48] Kyeyune, B. (**2017**). *Atomic Force Microscopy.* (Master Thesis), Lappeenranta University of Technology, African Institute for Mathematical Sciences.

[49] Zhang, H., Huang, J., Wang, Y., Liu, R., Huai, X., Jiang, J., Anfuso, C. (2018). Atomic force microscopy for two-dimensional materials: a tutorial review. *Optics Communications, 406*, 3-17.

[50] Wilson, R. A., Bullen, H. A. (**2006**). *Introduction to Scanning Probe Microscopy-Basic Theory-Atomic Force Microscopy (AFM).* Department of Chemistry. Northern Kentucky University.

[51] Singh, Y. (**2013**). Electrical Resistivity Measurements: A Review. *International Journal of Modern Physics: Conference Series, 22*, 745-756.

[52] Li, J. C., Wang, Y., Ba, D. C. (2012). Characterization of Semiconductor Surface Conductivity by Using Microscopic Four-Point Probe Technique. *Physics Procedia, 32*, 347-355.

[53] Chakraborty, M., Hashmi, M. S. J. (**2017**). An Overview of Biosensors and Devices. In *Reference Module in Materials Science and Materials Engineering*.

[54] Ali, J., Najeeb, J., Asim Ali, M., Farhan Aslam, M., Raza, A. (2017). Biosensors: Their Fundamentals, Designs, Types and Most Recent Impactful Applications: A Review. *Journal of Biosensors & Bioelectronics, 08*(01).

[55] Zuber, A. A., Klantsataya, E., Bachhuka, A. (**2019**). Biosensing. In *Comprehensive Nanoscience and Nanotechnology* (pp. 105-126).

[56] Kawamura, A., Miyata, T. (**2016**). Biosensors. In *Biomaterials Nanoarchitectonics* (pp. 157-176).

[57] Charych, D. H., Nagy, J. O., Spevak, W., Bednarski, M. D. (1993). Direct colorimetric detection of a receptor-ligand interaction by a polymerized bilayer assembly. *Science, 261*(5121), 585.

[58] Notingher, I. (2007). Raman spectroscopy cell-based biosensors. *Sensors, 7*(8), 1343-1358.

[59] Özden, A., Ay, F., Sevik, C., Perkgöz, N. K. (2017). CVD growth of monolayer MoS2: Role of growth zone configuration and precursors ratio. *Japanese Journal of Applied Physics, 56*(6S1), 06GG05.

[60] Fu, L., Sun, Y., Wu, N., Mendes, R. G., Chen, L., Xu, Z., Zhang, T., Rümmeli, M. H., Rellinghaus, B., Pohl, D., Zhuang, L., Fu, L. (2016). Direct Growth of MoS2/h-BN Heterostructures via a Sulfide-Resistant Alloy. *ACS Nano, 10*(2), 2063-2070.

[61] Zhan, Y., Liu, Z., Najmaei, S., Ajayan, P. M., Lou, J. (**2012**). Large-Area Vapor-Phase Growth and Characterization of MoS2 Atomic Layers on a SiO2 Substrate. *Small, 8*(7), 966-971.

[62] Li, H., Zhang, Q., Yap, C. C. R., Tay, B. K., Edwin, T. H. T., Olivier, A., Baillargeat, D. (2012). From Bulk to Monolayer MoS2: Evolution of Raman Scattering. *Advanced Functional Materials, 22*(7), 1385-1390.

[63] O'Brien, M., Scheuschner, N., Maultzsch, J., Duesberg, G. S., McEvoy, N. (2017). Raman Spectroscopy of Suspended MoS2. *physica status solidi (b), 254*(11), 1700218.

[64] Ling, X., Lee, Y.-H., Lin, Y., Fang, W., Yu, L., Dresselhaus, M. S., Kong, J. (2014). Role of the seeding promoter in MoS2 growth by chemical vapor deposition. *Nano letters, 14*(2), 464-472.

[65] Kim, M. S., Nam, G., Park, S., Kim, H., Han, G. H., Lee, J., Dhakal, K. P., Leem, J.-Y., Lee, Y. H., Kim, J. (2015). Photoluminescence wavelength variation of monolayer MoS2 by oxygen plasma treatment. *Thin Solid Films, 590*, 318-323.

[66] Mouri, S., Miyauchi, Y., Matsuda, K. (2013). Tunable Photoluminescence of Monolayer MoS2 via Chemical Doping. *Nano letters, 13*(12), 5944-5948.

[67] Diskus, M., Nilsen, O., Fjellvåg, H., Diplas, S., Beato, P., Harvey, C., Lantman, E. v. S., Weckhuysen, B. M. (**2012**). Combination of characterization techniques for atomic layer deposition MoO3 coatings: From the amorphous to the orthorhombic α-MoO3 crystalline phase. *Journal of Vacuum Science & Technology A, 30*(1), 01A107.

[68] Sharma, R. K., Reddy, G. B. (**2014**). Synthesis and characterization of α-MoO3 microspheres packed with nanoflakes. *Journal of Physics D: Applied Physics, 47*(6).

CURRICULUM VITAE

CEM ODACI
Electrical-Electronics & Industrial Engineer

E-mail : odacicem@gmail.com

Address : Yeni Bağlar District, Beraberlik Street, No.: 20/9 Tepebaşı/ESKİŞEHİR

Phone number : +90 536 996 43 72

PERSONAL INFORMATION

Date of Birth / Place : 01.12.1992 / Hatay

Marital Status : Single

Nationality : T.C.

Military Service : Completed

Gender : Male

Driver's License : None

EDUCATION

High School : Yüksel Acun Anadolu High School (2006-2010) (Degree: 89/100)

University : Anadolu University / Prepschool (English) (2010-2011)

University : Anadolu University / Electrical-Electronics Engineering(2011-2015) (Degree : 3.31/4) (Top student of the department)

University : Anadolu University / Industrial Engineering(2012/2016) (Double Major Degree : 3.24/4)

University : Eskişehir Technical University / Electrical-Electronics Engineering (Master Degree) (2016 - 2019)

Language : *English* : speaking (advance) – reading (advance) – writing (advance)

German : speaking (beginner)- reading (beginner)- writing (beginner)

Computer Skills : Ms Office (good), C programming (good) , Visual programming (good), GAMS (good), Matlab (good), C# programming (good), Autocad (beginner), ARENA (beginner), Assembly (good), Excel-VBA (MAKRO) (good)

PROJECTS

- Project of Hydrojen Gas-Powered Cars (HIDROANA, Shell Eco-Maraton Competition in Rotterdam in Holland, TUBITAK Alternative Energy Car Racing, 2012-2014)
- Project of Unmanned Air Vehicle (SUAS-Anadolu, 2013-2014)
- The Growth and Characterization of Graphene for Applications in the Supercapacitors (Dissertation Supported by TUBITAK-June 2015)

- Applications of 5S, Value Stream Mapping and SMED in a Sme Which Manufactures High Technology Aircraft Engine Parts (Dissertation-January 2016)

- Two dimensional (hetero)structures and electronic device applications (2016 – still)

- Novel, high-gain solid-state waveguide amplifiers for applications in backplane and inter-chip optical interconnects (TUBITAK project, 2016-2018)

- The application and verification of the innovative optimization methods inspired by the nature in potential development studies for single atomic layered MoS_2 and similar two-dimensional transition metal chalcogenites (TUBITAK project, 2018-still)

EXPERIENCES

- Representative of Substation of Eskişehir EMO-Youth Society(2012)
- President of Commision of Eskişehir EMO-Youth Society (2012)
- Shell Eco-Maraton Competition in Rotterdam in Holland (full cell-powered class) (2013)
- TUBITAK Alternative Energy Car Racing, Kocaeli (full cell-powered class) (Best Degree : 2) (2013)
- TUBITAK Alternative Energy Car Racing, Kocaeli (full cell-powered class) (2014)
- Member of TEMA Foundation (Fall-2014)

INTERNSHIP

Intern Engineer - Nanomagnetic Instruments Ltd. (15.06.2015-28.08.2015, Ankara, TURKEY)

Intern Engineer - AEP Anadolu Etap Penkon Tarım ve Gıda A. Ş. (27.05.2016-01.07.2016, Mersin, TURKEY)

Intern Engineer - Elginay Otomotiv San. Ve Tic. Ltd. Şti. (18.07.2016-12.08.2016, Mersin, TURKEY)

ADDITIONAL INFORMATION

Conferences:

* PHOTONICS 2017, National Optics, Electro-optics and Photonics Workshop, 29 September 2017, Istanbul

* 2017 IEEE Photonics Conference, 30th Annual Conference of the IEEE Photonics Society, 1 - 5 October 2017, Hilton Orlando Lake Buena Vista, Florida

* 13^{th} Nanoscience & Nanotechnology Conference, 22-25 October 2017, Antalya, Turkey

Publications:

* Time Dependent Structural Analysis of CVD Grown MoS_2 Flakes with Different Configurations, *International Conference on Solid State Devices and Materials*, **2017** (Conference paper)

* Control of Optical Amplification Process with Extremely Low Background Loss in Er:Al_2O_3 Waveguides, *IEEE Photonics Conference (IPC)*, **2017** (Conference paper)

* Low Loss Atomic Layer Deposited Al2O3 Waveguides for Applications in On-chip Optical Amplifiers, *IEEE Journal of Selected Topics in Quantum Electronics*, **2018** (Article)

* Glass-Assisted CVD Growth of Large-Area MoS_2,WS_2 and $MoSe_2$ Monolayers on Si/SiO_2 Substrate, *Materials Science in Semiconductor Processing*, **2019** (Accepted article)